NAVAL POSTGRADUATE SCHOOL

MONTEREY, CALIFORNIA

THESIS

ACOUSTIC COMMUNICATIONS CONSIDERATIONS FOR COLLABORATIVE SIMULTANEOUS LOCALIZATION AND MAPPING

by

Ryan Peter Hilger

December 2014

Thesis Advisor:	Douglas Horner
Second Reader:	Noel DuToit

THIS PAGE INTENTIONALLY LEFT BLANK

REPORT DOCUMENTATION PAGE		Form Approved OMB No. 0704–0188

1. AGENCY USE ONLY *(Leave blank)*	2. REPORT DATE December 2014	3. REPORT TYPE AND DATES COVERED Master's Thesis

4. TITLE AND SUBTITLE ACOUSTIC COMMUNICATIONS CONSIDERATIONS FOR COLLABORATIVE SIMULTANEOUS LOCALIZATION AND MAPPING	5. FUNDING NUMBERS
6. AUTHOR(S) Ryan Peter Hilger	
7. PERFORMING ORGANIZATION NAME(S) AND ADDRESS(ES) Naval Postgraduate School Monterey, CA 93943-5000	8. PERFORMING ORGANIZATION REPORT NUMBER
9. SPONSORING /MONITORING AGENCY NAME(S) AND ADDRESS(ES) N/A	10. SPONSORING/MONITORING AGENCY REPORT NUMBER

11. SUPPLEMENTARY NOTES The views expressed in this thesis are those of the author and do not reflect the official policy or position of the Department of Defense or the U.S. Government. IRB Protocol number _____N/A_____.

12a. DISTRIBUTION / AVAILABILITY STATEMENT Approved for public release; distribution is unlimited.	12b. DISTRIBUTION CODE

13. ABSTRACT (maximum 200 words)

This thesis considers the use of acoustic communications in reducing position uncertainty for collaborating autonomous underwater vehicles. The foundation of the work relies on statistical techniques for accurate navigation without access to GPS, known as Simultaneous Localization and Mapping (SLAM). Multiple AUVs permit increased coverage, system redundancy and reduced mission times. Collaboration through acoustic communications can minimize navigational uncertainty by permitting the group to benefit from locally discovered information. However, the propagation of acoustic communications can be used to counter detect the system during naval operations.

The thesis gives explicit consideration to tactical security in acoustic communications for a multi-AUV SLAM system. It provides initial techniques and analysis for minimizing communications between AUVs. The reduction is accomplished through a statistical method that allows for the estimation of the updated covariance matrices. Normally, SLAM techniques use expropioceptive (sonar and cameras) sensors and computer vision algorithms for the detection and tracking of navigational references. We propose a novel use of the acoustic modem as another sensor. It leverages the physical characteristics of underwater acoustic transmissions and the information transmitted in the signal to provide an additional measurement. We believe this is the first emphasis on minimizing communications within a multi-vehicle SLAM approach.

14. SUBJECT TERMS UUV, AUV, SLAM, simultaneous localization and mapping, position uncertainty, navigation, minefield, mapping, tactical security, GPS, area denial, anti-access, A2/AD, acoustic communications, Bayesian inference	15. NUMBER OF PAGES 103
	16. PRICE CODE

17. SECURITY CLASSIFICATION OF REPORT	18. SECURITY CLASSIFICATION OF THIS PAGE	19. SECURITY CLASSIFICATION OF ABSTRACT	20. LIMITATION OF ABSTRACT
Unclassified	Unclassified	Unclassified	UU

NSN 7540–01-280-5500

Standard Form 298 (Rev. 2–89)
Prescribed by ANSI Std. 239–18

THIS PAGE INTENTIONALLY LEFT BLANK

Approved for public release; distribution is unlimited

ACOUSTIC COMMUNICATIONS CONSIDERATIONS FOR COLLABORATIVE SIMULTANEOUS LOCALIZATION AND MAPPING

Ryan Peter Hilger
Lieutenant, United States Navy
B.A., University of Kansas, 2007

Submitted in partial fulfillment of the
requirements for the degree of

MASTER OF SCIENCE IN MECHANICAL ENGINEERING

from the

NAVAL POSTGRADUATE SCHOOL
December 2014

Author: Ryan Peter Hilger

Approved by: Dr. Douglas Horner
Thesis Advisor

Dr. Noel DuToit
Second Reader

Dr. Garth Hobson
Chair, Department of Mechanical and Aerospace Engineering

THIS PAGE INTENTIONALLY LEFT BLANK

ABSTRACT

This thesis considers the use of acoustic communications in reducing position uncertainty for collaborating autonomous underwater vehicles. The foundation of the work relies on statistical techniques for accurate navigation without access to GPS, known as Simultaneous Localization and Mapping (SLAM). Multiple AUVs permit increased coverage, system redundancy and reduced mission times. Collaboration through acoustic communications can minimize navigational uncertainty by permitting the group to benefit from locally discovered information. However, the propagation of acoustic communications can be used to counter detect the system during naval operations.

The thesis gives explicit consideration to tactical security in acoustic communications for a multi-AUV SLAM system. It provides initial techniques and analysis for minimizing communications between AUVs. The reduction is accomplished through a statistical method that allows for the estimation of the updated covariance matrices. Normally, SLAM techniques use expropioceptive (sonar and cameras) sensors and computer vision algorithms for the detection and tracking of navigational references. We propose a novel use of the acoustic modem as another sensor. It leverages the physical characteristics of underwater acoustic transmissions and the information transmitted in the signal to provide an additional measurement. We believe this is the first emphasis on minimizing communications within a multi-vehicle SLAM approach.

THIS PAGE INTENTIONALLY LEFT BLANK

TABLE OF CONTENTS

I. INTRODUCTION....1
- **A. MOTIVATION....1**
- **B. PROBLEM STATEMENT....2**
- **C. APPROACH....3**

II. ACOUSTIC COMMUNICATIONS AND RANGING....5
- **A. MODIFIED REMUS-100 AUV....5**
  - **1. Kearfott KN-6051 SEADeViL INS....7**
  - **2. WHOI Acoustic Micromodem....7**
  - **3. Teledyne BlueView FL450X FLS....8**
- **B. SOUND PROPAGATION IN THE OCEAN....8**
  - **1. Overview....8**
  - **2. Sound Speed....8**
  - **3. Sound Propagation in the Ocean....9**
  - **4. The Passive Sonar Equation....13**
  - **5. Spreading and Absorption....14**
  - **6. Losses at the Boundary Layer....15**
- **C. ACOUSTIC RANGING, ONE WAY TRAVEL TIME....16**

III. SIMULTANEOUS LOCALIZATION AND MAPPING....19
- **A. INTRODUCTION....19**
  - **1. Position Uncertainty in Robotics....19**
  - **2. Sources of Uncertainty....20**
  - **3. SLAM as a Stochastic Process....21**
  - **4. Optimal Estimation....25**
- **C. INCREMENTAL SMOOTHING AND MAPPING....26**
  - **1. Process and Measurement Models....26**
  - **2. Linearization....27**
  - **3. Variable Reordering....28**
  - **4. Process Results....28**
  - **5. Mathematical Example....29**

IV. COLLABORATIVE MULTIPLE AUV SLAM....35
- **A. RECENT WORK....35**
  - **1. Centralization and Hierarchy....35**
  - **2. Beacon-Aided SLAM....36**
  - **3. Behaviors and Cooperative SLAM....36**
  - **4. Dynamic Features in SLAM....37**
- **B. PROPOSED APPROACH....37**
- **C. INFERRING COVARIANCE....38**
  - **1. The Bayesian Inference....38**
    - ***a. A Numerical Example....39***
  - **2. Value of Acoustic Communications and Ranging....41**
    - ***a. Numerical Example Revisited....43***

b. Determining Relative Performance 44
c. Aspect Dependence 45
D. ALGORITHM DEVELOPMENT AND INTEGRATION 48
1. System Representation and Objectives 48
2. Measuring Covariance Growth and the Broadcasting Threshold 50
3. Threshold for an Informed Reply 51
4. Acoustic Message Construction and Packet Loss 52
5. Covariance Reduction 53
6. Reintegration with iSAM2 53
V. SIMULATION AND ANALYSIS 55
A. OVERVIEW 55
B. EXPERIMENTAL CONSTRUCTION 55
1. Operational Area 55
2. Simulation Variables 57
3. Measures of Effectiveness and Performance 59
4. Simulation Plan 59
C. SIMULATION CONSTRUCTION 60
1. Performance Baseline Determination 60
2. Threshold Determination 63
D. RESULTS AND PERFORMANCE ANALYSIS 65
1. Performance Baseline Determination 65
2. Broadcast-Reply Performance 70
E. VALUE OF ACOUSTIC COMMUNICATIONS 72
VI. CONCLUSIONS AND FUTURE RESEARCH 75
A. CONCLUSIONS 75
1. Major Results 75
2. Contributions 75
3. Limitations and Issues 76
B. FUTURE WORK 76
C. APPLICATIONS 77
APPENDIX A: SOUND SPEED EQUATION CONSTANTS 79
LIST OF REFERENCES 81
INITIAL DISTRIBUTION LIST 85

LIST OF FIGURES

Figure 1. Two NASA astronauts hold the NPS-modified REMUS 100 AUV during a photo opportunity at the Aquarius Reef Base during the NEEMO mission off the coast of Key Largo, Florida, in September 2013. 6

Figure 2. Depiction of Snell's Law where c_1 and c_2 are the sound speeds in the given water layer and θ_1 and θ_2 are the grazing angles of the acoustic rays from the horizontal plane dividing the two water layers in question. 10

Figure 3. A collection of sound propagation plan views for varying sound speed profiles, from [11]. 11

Figure 4. On the left (a), the canonical Munk sound speed profile, ending at 100 meters depth. On the right (b), the ray trace diagram from a source radiating omni-directionally in (a) at 30 meters depth with no accounting for transmission losses. The red and blue rays simply indicate whether the initial transmission angle was above or below the horizontal plane [12]. 12

Figure 5. The robot, with a finite PUC, senses a landmark and takes a sensor measurement. The uncertainty of the feature and the AUV are the blue ellipse and red circle, respectively. 22

Figure 6. The robot, with an updated PUC, has moved a fixed distance and takes a measurement of the same landmark. The initial PUC is in light red for comparison. 23

Figure 7. After two measurements of the same landmark, the robot's PUC, the red ellipse is substantially smaller than it was at the beginning. The initial ellipse is in light red to show the reduction. The updated uncertainty of the feature is shown as the light blue ellipse, and is markedly smaller than the initial, shown in dark blue. 24

Figure 8. The example problem from Section III.A.3 now with a coordinate system overlaid. 29

Figure 9. AUV position after one 25-second time step. The AUV has detected the feature at [50,10] and made the pose to landmark constraint in iSAM2. 30

Figure 10. The visual sparsity pattern of the A matrix after a single 25-second time step with one feature detected. 31

Figure 11. The visual sparsity pattern of the R matrix following QR factorization of the A matrix. Some of the entries may have changed during QR factorization as a result of applying Givens rotations to specific entries in the lower half of the A matrix. 31

Figure 12. *A priori* 95% confidence ellipses for two AUVs centered at the origin in (a) and after the mathematical integration of the two through a Bayesian inference in (b) with the updated 95% ellipse shown in magenta. 41

Figure 13. (a) The inferential results of two orthogonal, 95% ellipses as compared to (b) two collinear, 95% ellipses. The updated covariance matrix in (a) showed significant reduction (~93% by matrix norm) whereas the reduction in (b) is much more modest (66% by matrix norm) and still exhibits greater directional uncertainty in the x-direction. 47

Figure 14. A schematic representation of the proposed algorithm to reduce position uncertainty through acoustic communications with an emphasis on tactical security concerns in Steps 3 and 4. 49
Figure 15. A satellite image of the public marina in Monterey Bay, California, with hypothetical vehicle tracks overlaid. 56
Figure 16. A map of the simulated search environment with the navigation tracks for 4 AUVs overlaid. The red tracks indicate a search in progress. Each of the four labeled quadrants has a different feature density. The feature density will be varied across simulations. 57
Figure 17. The simulation plot with varying feature densities by quadrant. Quadrant 1 is featureless, Quadrant 2 has 6 features, Quadrant 3 has 12 features, and Quadrant 4 has 18 features. 62
Figure 18. The simulation plot with varying feature densities by quadrant. Quadrant 1 has 24 features, Quadrant 2 has 30 features, Quadrant 3 has 36 features, and Quadrant 4 has 42 features. 63
Figure 19. The simulation plot for the threshold evaluation with the given feature densities. Quadrant 1 is featureless, Quadrant 2 has 12 features, Quadrant 3 has 30 features, and Quadrant 4 has 42 features. 64
Figure 20. The rms average of the time-indexed covariance matrix norms for six GPS fix intervals: 15, 30, 45, 60, 90, and 120 minutes. The values converge or begin to show convergence to the predicted analytical solutions for the rms average of a sawtooth wave. 66
Figure 21. Average covariance matrix norms from 12 simulation runs in each of eight different feature densities. 67
Figure 22. The rms average value of the covariance matrix norms from 12 simulations runs in each of eight different feature densities. 67
Figure 23. The rms average values of the covariance matrix norms for four feature densities and four GPS fix intervals. The feature densities are 6, 18, 30, and 42 square kilometers and the GPS fix intervals are 30, 60, 90, and 120 minutes. This figure defines the performance trade space for a reply threshold determination. 68
Figure 24. Average number of acoustic transmissions by possible percent reduction threshold value for each AUV. The average is across three simulations for each threshold value. 70
Figure 25. Average percent reduction from acoustic communications by possible percent reduction threshold value. The average is across three simulation runs at each threshold value. In poorly featured environments (red and blue lines), the trend is clear. In modest to well-featured environments (magenta line), the small number of simulations did not smooth the data sufficiently to draw conclusions. The black line represents the fourth AUV, which did not communicate. 71
Figure 26. RMS average values of the time-indexed covariance matrix norms for four AUVs using a broadcast-reply acoustic communications scheme with a 20 percent possible reduction reply threshold. 72

LIST OF TABLES

Table 1. Specifications and operating characteristics of the NPS-modified Hydroid REMUS-100 AUV with the BlueView forward looking sonar and cross body thrusters attached. 6

Table 2. The major terms of the sonar equation and their definitions [9], [10]. 13

Table 3. The independent simulation control variables as related to determining the performance of acoustic communications in MVSLAM operations. 58

Table 4. The assignment of feature densities and GPS fix intervals for the first two sets of simulation runs. The runs will collect the performance metrics necessary to define the trade space for SLAM operations. 61

Table 5. The fixed simulation parameters of feature density, by quadrant, and GPS fix interval for the threshold determination runs. 64

THIS PAGE INTENTIONALLY LEFT BLANK

LIST OF ACRONYMS AND ABBREVIATIONS

A2/AD	Anti-Access/Area Denial
ADCP	Acoustic Doppler Current Profiler
AUV	Autonomous Underwater Vehicle
CEP	Circular Error Probable
COLAMD	Column approximate minimum degree
CTD	Conductivity-Temperature-Depth
dB	Decibels
DVL	Doppler Velocity Log
EIF	Extended Information Filter
EKF	Extended Kalman Filter
FLS	Forward Looking Sonar
GPS	Global Positioning System
i.i.d.	Independent, Identically Distributed
INS	Inertial Navigation System
iSAM2	Second-Generation Incremental Smoothing and Mapping
kHz	Kilohertz
LLS	Linear Least Squares
m/s	Meters per second
MAP	Maximum a Priori
MLE	Maximum Likelihood Estimator
MOE	Measure of Effectiveness
MOP	Measure of Performance
MVSLAM	Multiple Vehicle SLAM
NASA	National Aeronautics and Space Administration
NEEMO	NASA Extreme Environments Mission Operations
NLLS	Non-Linear Least Squares
NPS	Naval Postgraduate School
OWTT	One-Way Travel Time

P	Pressure
PPT	Parts per Thousand
PUC	Position Uncertainty
rms	Root Mean Square
RPM	Revolutions Per Minute
S	Salinity
SLAM	Simultaneous Localization and Mapping
SQIM	Square Root Information Matrix
SSG	Strategic Studies Group
T	Temperature
TDMA	Time Domain Multiple Access
TDOA	Time Difference of Arrival
TL	Transmission Loss
TOA	Time of Arrival
TOF	Time of Flight
TOT	Time of Transmission
USBL	Ultra Short Baseline
UUV	Unmanned Underwater Vehicle
WHOI	Woods Hole Oceanographic Institute

ACKNOWLEDGMENTS

Writing this thesis laid the groundwork for a much broader journey of intellectual discovery on the confluence of military operations and new technology, complete with the frustrating pitfalls that arrest progress. The two years spent researching, coding, and writing this thesis led me to some outstanding individuals, whose guidance helped shape my assumptions and challenged my thinking.

To both Dr. Daphne Kapolka and Dr. John Colosi, I owe my sincere thanks for your feedback and education on ocean acoustics. Your willingness to help me through this is a testament to your dedication and professionalism.

Early in my tour at NPS, I was encouraged to seek out Dr. Timothy Chung as one of the leading robotics experts on campus. I am happy that I did, for I came away from all of our conversations over the previous two years with new insights and motivation to attack the problem. I am very thankful for your wisdom and help.

Dr. Doug Horner. This point has been a long time in coming, but your steadfast focus on the operational research objective enabled me to keep focus on what really mattered. Thank you for a great two years and for all the tangential conversations that followed our meetings.

The Chief of Naval Operations Strategic Studies Group (SSG) provided a two-fold contribution. It fundamentally altered how I approach and think about problems and provided a retrospectively necessary break from this thesis that allowed me to approach this problem anew. The sweeping course change that became this thesis came out of the phenomenal discussions, never related to this work, with my cohort in SSG XXXIII. For more reasons than that do I owe them my sincere thanks and gratitude.

Rear Admiral Jerry Ellis. Your feedback on keeping this work operationally relevant was of inestimable value. Beyond that, your friendship and mentorship has led this tour of duty to be what I imagine will be a seminal point in my career. Words cannot express how thankful I am for knowing you.

Finally, to my wife, Heather. The success I have enjoyed in my career is all because of your steadfast love and support. I would not be the husband, father, or officer that I am today without you. The continual refrain of “I have homework” finally comes to an end. Our next adventure together awaits!

I. INTRODUCTION

A. MOTIVATION

Few naval powers possess the ability to challenge the United States Navy in deep water or effectively deny us access to anywhere we wish to sail. The rise of cheap, effective, asymmetric anti-access and area denial (A2/AD) systems represents the best possible solution to denying the United States access to a region without the need to be able to conventionally confront maritime forces in Mahanian naval combat. The United States experienced this problem first hand on April 14, 1988, when the USS Samuel B. Roberts (FFG 58) struck a mine in the Persian Gulf while escorting tankers as part of Operation Earnest Will. The subsequent transport back to the United States and repairs cost taxpayers $89.5 million [1].

The mere threat of a naval minefield can effectively stop maritime traffic and commerce in a port or strategic chokepoint, such as the Strait of Hormuz where the USS Samuel B. Roberts was operating. The low cost and advancing technology of naval mines makes them particularly well-suited for A2/AD applications. The United States must possess the ability to rapidly and covertly map and neutralize a minefield in order to assure access and ensure the free flow of maritime trade in the global commons. The present means of mine countermeasures largely reside on surface ships and are neither covert nor rapid. Autonomous underwater vehicles (AUV) have the ability to map the environment in a covert manner that does not necessarily require an overt presence. They do not require real time human control and are difficult to detect. Multiple AUVs permit a wider area to be searched and mapped more efficiently than any present means. The use of multiple AUVs will be required to keep minefield mapping and clearance both covert and efficient. At present, the use of AUVs in minefield mapping is in its infancy and AUVs lack the ability to collaboratively complete a mission; each vehicle would operate essentially independently. Recent research has enabled multiple AUVs to begin coordinating their efforts. This body of research has significant operational value for undersea operations.

B. PROBLEM STATEMENT

The underwater environment presents significant challenges to both navigation and localization since the vehicles must operate without the benefit of the global positioning system (GPS). This environment necessitates a more accurate means of navigation for AUVs to ensure that they can remain underwater and undetected. Obtaining a GPS fix for an AUV is a highly inefficient part of the overall mission profile as it necessitates the AUV rising from deep water, loitering on the surface where the threat of collision or counter-detection is greater, submerging back to its programmed search depth, and reacquiring its position with respect to the underwater environment. Underwater beacon systems have been developed and fielded, but deployment of these beacon fields requires both prior warning and time that may not be available. AUVs must have the ability to localize their position without the need for external navigation aids. The development of simultaneous localization and mapping (SLAM) [2] allowed autonomous vehicles to both localize their position and map their environment at the same time. This field provides a major operational capability for accurate underwater navigation and mapping. Many of the Navy's undersea warfare missions would benefit from advances in SLAM, including mine countermeasures. Research into SLAM algorithms has exploded in recent years as researchers and end users search for a way to make these robots reliant on their onboard systems only and make them more capable to accurately navigate in difficult terrain and environments. However, only a small percentage of the field has tried to solve the problems of multiple AUV coordination in a SLAM environment. Collaborative SLAM between multiple AUVs permits improved coverage, greater accuracy, and faster, more efficient operations. In the given minefield mapping scenario under current employment constructs, a fleet of AUVs tasked to map a minefield would be operating in the same space, but independently. The reduction of their position uncertainty from either SLAM or a GPS fix cannot be shared with other vehicles for their benefit. The ability for a single AUV to share its position, or state, information following a reduction in its position uncertainty, whether through a GPS fix or through SLAM, with the other AUVs conducting SLAM operations would prolong

submerged operations and minimize disruptions to mapping operations while potentially improving the overall quality of the maps produced.

This thesis will consider the role of acoustic communications in multiple-AUV operations. Multiple-AUV SLAM (MVSLAM) is the ability for multiple AUVs to simultaneously conduct SLAM operations and share their information with other AUVs to improve the overall performance of the group. This thesis will explore the value of acoustic communications to MVSLAM in reducing position uncertainty, and tangentially, map accuracy. Since the acoustic communications present a real threat to counter-detection, this thesis will heuristically balance performance improvements with tactical security considerations. It will explore strategies for minimizing communications while maintaining navigational accuracy.

Tactical security concerns, an issue unique to the military, will underpin this thesis to ensure that the developed solution keeps with the strong desire to remain covert and undetected. This viewpoint is conspicuously absent from the present body of research and will be a major contribution to it. Current approaches rely on frequent communication between vehicles to pass information; whether it is position information, maps, or command and control functions is immaterial. The frequencies of the acoustic modems used in this thesis will propagate, under typical sound conditions, omni-directionally for several kilometers and correspond to frequencies that active sonar intercept receivers can detect. Minimizing the number of messages required to be transmitted and the intervals at which they need to be transmitted directly correlate with a reduction in the probability of counter-detection.

C. APPROACH

The overall objective of this thesis is to adapt the Second Generation Incremental Smoothing and Mapping (iSAM2) algorithm [3] for use in multiple-AUV SLAM. To accomplish this, this thesis will be organized as follows. Chapter II will describe the equipment used in this research and review the literature of sound propagation in seawater and acoustic ranging and localization methods. Chapter III will review current approaches to MVSLAM, the fundamental mathematics behind position uncertainty in

robotics, and provide a detailed description of iSAM2. Chapter IV will discuss the development of a hybrid approach to MVSLAM using the mathematical concept of a Bayesian inference coupled with a novel use of acoustic communications to reduce position uncertainty. We will show that this solution can be applied to *n*-number of AUVs. Chapter V will validate these changes through simulation, along with an exploration of the value of acoustic communications to MVSLAM. Tactical security considerations will be heuristically incorporated. Chapter VI will discuss the major results, contributions, and conclusions from this work, as well as propose significant areas for future work.

II. ACOUSTIC COMMUNICATIONS AND RANGING

Communication is fundamental to the success of MVSLAM operations. In the underwater environment, only acoustic communications have the necessary range to enable communications between vehicles. Underwater communication is challenging because of the highly uncertain nature of sound propagation, the low data rate in the communications channel, and the significant losses the signal incurs during interactions with water molecules. Despite these challenges, understanding how acoustic rays propagate through the water provides information that can be used in improving navigational accuracy. This section will discuss the equipment used in this thesis, the propagation of sound in the ocean, and a method of acoustic ranging.

A. MODIFIED REMUS-100 AUV

This thesis exclusively utilizes the Hydroid REMUS-100 AUV for SLAM operations. NPS owns two REMUS AUVs and has modified them extensively to support various research aims. This section will detail both the general characteristics of the REMUS 100 AUV as well as the specific modifications that NPS has made to the vehicles. Figure 1 shows the NPS REMUS AUV during a photo opportunity during the National Aeronautics and Space Administration (NASA) Extreme Environments Mission Operations (NEEMO) off the coast of Key Largo, Florida, in September 2013. The mission used the REMUS vehicles to map a simulated asteroid environment and a tethered hovering AUV as a guidance and astronaut-assistance platform.

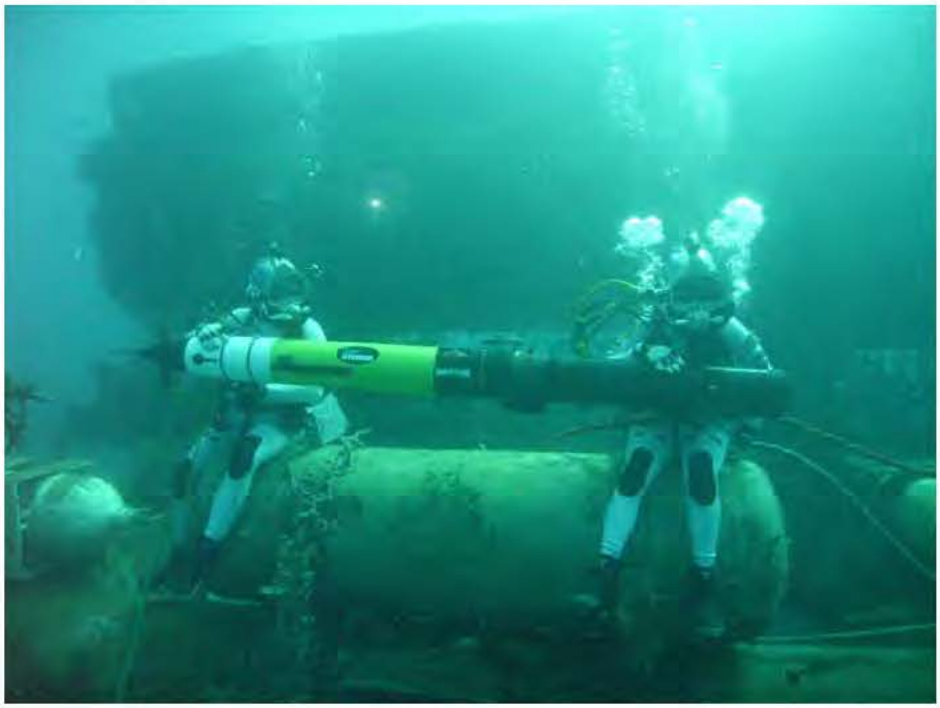

Figure 1. Two NASA astronauts hold the NPS-modified REMUS 100 AUV during a photo opportunity at the Aquarius Reef Base during the NEEMO mission off the coast of Key Largo, Florida, in September 2013.

The REMUS 100 is a man-portable, lightweight AUV designed primarily for survey-type operations. Table 1 outlines the basic specifications.

Table 1. Specifications and operating characteristics of the NPS-modified Hydroid REMUS-100 AUV with the BlueView forward looking sonar and cross body thrusters attached.

Specifications of the REMUS-100 AUV	
Length	Approx. 8 ft
Diameter	7.5 in
Weight	95 lbs
Maximum Depth	100 m
Speed	Up to 4.5 kts
Endurance	8-10 hours

The REMUS 100 is a highly modular system that can be easily customized to complete a wide variety of underwater tasks. For the type of research that NPS conducts with these vehicles, we have the following sensors and systems installed:

- Kearfott KN-6051 SEADeViL inertial navigation system (INS) with a Doppler Velocity Log (DVL) and GPS
- Fore and aft cross-body thrusters from Hydroid
- Woods Hole Oceanographic Institute (WHOI) Acoustic Micromodem
- YSI CT-600-XL Conductivity-Temperature-Depth (CTD) Sensor
- Marine Sonic Technology, Ltd. Side Scan Sonar
- Teledyne BlueView MB2250 3D Microbathymetry Sonar
- Teledyne BlueView FL450X 2D Forward Looking Sonar (FLS)
- Acoustic Doppler Current Profiler (ADCP)

The remainder of this section will describe the INS, acoustic modem, and forward looking sonar in greater detail since they are fundamental to this thesis.

1. Kearfott KN-6051 SEADeViL INS

The KN-6051 is a military-grade INS that combines inputs from onboard sensors, such as the DVL, with external measurements from GPS when they can be acquired. The ring laser gyro-based system has an overall accuracy of 0.5% error per unit distance traveled. This equates to a 5-meter error per kilometer. This error is in terms of the circular error probable (CEP) rate, which translates to a 50% probability of being within that circle. For heading, the INS is accurate to 5 mils, or 0.28 degrees. The GPS, with DVL aiding, is only accurate to a 10-meter CEP [4]. However, since it is an external position source, it is a community standard practice to assume no error in that position and take it as truth.

2. WHOI Acoustic Micromodem

WHOI developed this acoustic micromodem for their research purposes and it has quickly become an industry-leading piece of equipment. The device requires very little power. It idles and receives at approximately 158 mW on the 12V system, and requires less than 100 W for a five second burst transmission—very low power. The modem

transmits at approximately 25 kHz. Acoustic communications in seawater are very low data rate channels compared to electromagnetic or radio communications in air, and are on the order of bytes to a few kilobytes per second [5].

3. Teledyne BlueView FL450X FLS

The sonar systems installed come as a specially-engineered module from Teledyne BlueView to include both the FLS and microbathymetry sonar in the same housing. Since this thesis does not require the use of microbathymetry information, we will discuss only the performance of the FL450X FLS. The sonar operates at 450 kHz and has a field of view of 130 degrees horizontally and 45 degrees vertically. The sonar can detect objects in this field of view out to 280 meters, but between 5–100 meters is optimal. The object detection software supplied with the sonar can detect objects with an accuracy of 1 m in the range direction and 1.2 degree accuracy in bearing [6].

B. SOUND PROPAGATION IN THE OCEAN

1. Overview

The ocean is an incredibly complex environment and sound propagation in the ocean can be exceedingly difficult to model and predict. Simplifications and assumptions about sound propagation in one area of the world may not hold true for another area simply based on physical conditions such as bottom type, presence of biological organisms, salinity content, and more. However, basic models of sound propagation and sound speed equations will function adequately over the limited physical ranges that multiple-AUV SLAM will encompass. This section will discuss the basic mechanisms of sound propagation, the factors that influence sound speed, and the factors affecting transmission loss from a radiated source.

2. Sound Speed

Three principle factors govern sound speed in water: salinity, pressure, and temperature. In the littoral waters where minefields would likely be placed, salinity and temperature dominate the sound speed profile. Pressure does not normally affect the change in sound speed until the depth is below the main thermocline, which generally

occurs only in deep water. Several researchers have attempted to create an equation to predict the speed of sound in seawater. The equation developed by Del Grosso [7] and updated by Dushaw et al. [8]7 has been accepted as the most accurate and useable equation by the acoustics community. Equation (2.1) shows the Del Grosso equation with the modifications from [8]. The numerical constants (C_{xx}) for each term are provided in Appendix A. The physical properties are measured in degrees Celsius for temperature (T), parts per thousand (ppt) for salinity (S), and kg/cm^2 (gauge) for pressure (P).

$$\begin{aligned} C_{STP}[m/s] &= C_{000} + \Delta C_T + \Delta C_S + \Delta C_P + \Delta C_{STP} \\ C_{000} &= 1402.392 \\ \Delta C_T &= C_{T1}T + C_{T2}T^2 + C_{T3}T^3 \\ \Delta C_S &= C_{S1}S + C_{S2}S^3 \\ \Delta C_P &= C_{P1}P + C_{P2}P^2 + C_{P3}P^3 \\ \Delta C_{STP} &= C_{TS}TS + C_{TP}TP + C_{T2P2}T^2P^2 + C_{TP2}TP^2 + C_{TP3}TP^3 + \ldots \\ & \quad C_{T3P}T^3P + C_{S2P2}S^2P^2 + C_{T2S}T^3S + C_{TS2P}TS^2P + C_{TSP}TSP \end{aligned} \tag{2.1}$$

The equation performs extremely well in both deep and shallow water. Reported accuracy, verified in [8], shows the equation to be accurate to within 0.3 meters per second (m/s) with a standard deviation of 0.05 m/s across the range of likely input values for temperature, salinity, and pressure. Equation (2.1) will be used onboard the REMUS vehicle to calculate sound speed as sensor measurements become available for the purpose of acoustic ranging.

3. Sound Propagation in the Ocean

In an isovelocity sound profile, sound propagates linearly and spreads in a spherical manner until it interacts with a boundary layer, such as the air-ocean or ocean-bottom interfaces. However, isovelocity sound profiles are unlikely to exist in a dynamic ocean environment; and therefore, the sound propagates in a curvilinear manner, refracting incrementally as governed by Snell's Law, given below in Equation (2.2), where c is the sound speed in a given layer and θ is incident angle of the sound ray [9], [10]. The curvilinear behavior results from incremental changes in temperature, pressure,

and salinity in the vertical water column, as a qualitative examination of Equation (2.1) shows.

$$\frac{\cos\theta_1}{c_1} = \frac{\cos\theta_2}{c_2} \tag{2.2}$$

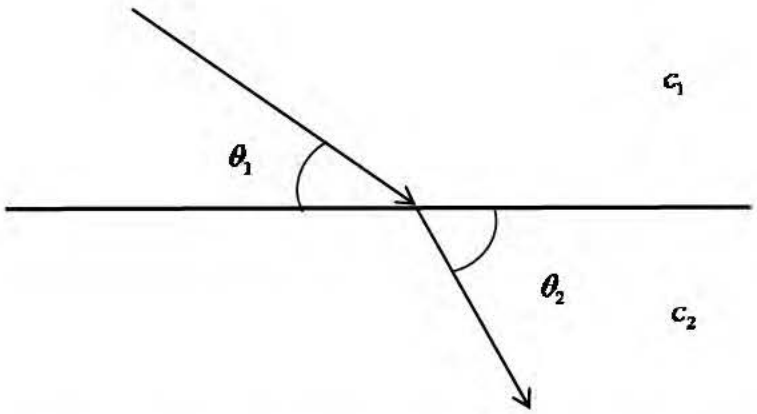

Figure 2. Depiction of Snell's Law where c_1 and c_2 are the sound speeds in the given water layer and θ_1 and θ_2 are the grazing angles of the acoustic rays from the horizontal plane dividing the two water layers in question.

Figure 2 and Equation (2.2) show the relationship between how changes in the speed of sound in the vertical water column produce curvilinear ray propagation. Figure 3 shows how sound propagates horizontally for several non-isovelocity sound speed profiles.

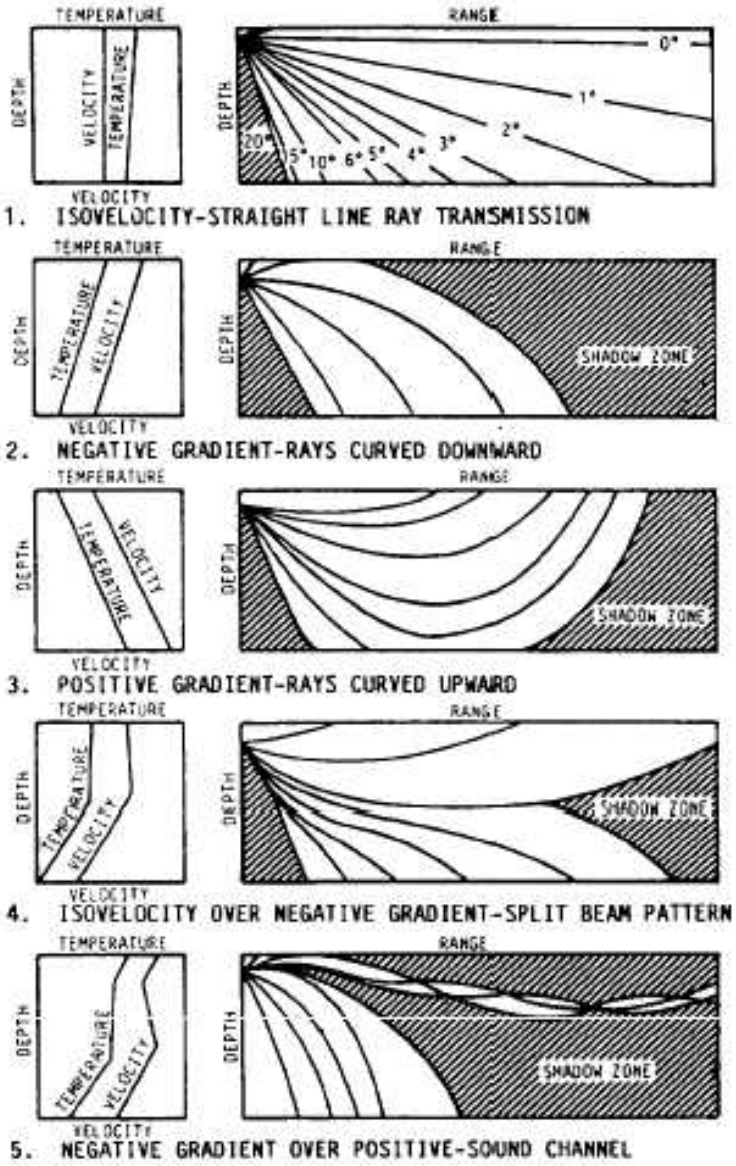

Figure 3. A collection of sound propagation plan views for varying sound speed profiles, from [11].

Over the ranges that AUVs with the WHOI acoustic modem can communicate, the propagation paths will be either curvilinear direct path, with no boundary interactions, as would likely be the case in deep water, or will reflect off the bottom, surface, or both, resulting in greater losses and shorter ranges, as we would expect in a very shallow water littoral environment. Snell's Law provides a convenient way of thinking about sound

propagation at the conceptual level, but the formula does not capture sufficiently the complexity of the propagation. The differential equation form, independent of frequency, can be iteratively solved through computer-based numerical methods, such as finite element analysis.

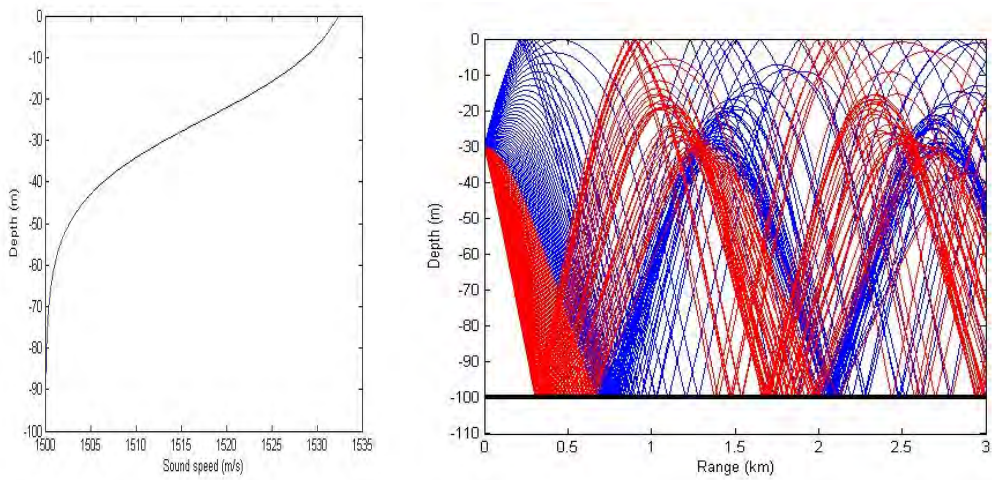

Figure 4. On the left (a), the canonical Munk sound speed profile, ending at 100 meters depth. On the right (b), the ray trace diagram from a source radiating omni-directionally in (a) at 30 meters depth with no accounting for transmission losses. The red and blue rays simply indicate whether the initial transmission angle was above or below the horizontal plane [12].

Figure 4 shows how busy the acoustic picture can become with an omnidirectional source radiating in the ocean at a given depth. Each ray shown is an individual ray transmitted from the source at a specified angle. The sum of these rays reflects the behavior of an omnidirectional source. The ray traces provide no information regarding the strength of the acoustic signal at any point since transmission loss varies with multiple parameters. Since the degradation of an acoustic signal and the length of time it takes to propagate from the source to the receiver are of vital interest to this thesis, a discussion of the sonar equation and its subordinate loss terms is therefore warranted. Additionally, Figure 4 provides an initial insight into the uncertainty that we face in developing acoustic ranging equations, given the inability to know which ray we received, how that particular ray interacted with the ocean bottom and surface, or how the

local effects of the seawater it passed through affected it, to name a scant few of the variables at play here.

4. The Passive Sonar Equation

In its simplest form, the passive sonar equation relates the received signal level to the level required for signal detection and is generally reported in decibels (dB), referenced to 1 μPa in seawater.[1] From source to operator, the signal undergoes a number of losses. For ease of representation, we present them in a tabular format in Table 2.

Table 2. The major terms of the sonar equation and their definitions [9], [10].

Parameter Symbol	Description
SL	Source level: the radiated intensity of the acoustic source, referenced to 1 yard from the source, by convention.
TL	Transmission losses: includes spreading and attenuation, one-way
NL	Noise level: includes ambient and self-noise at the receiver
DI	Directivity index: the ability of the array to detect the signal
DT	Detection threshold: the ability of the system to detect the signal

[1] All signal values in the remainder of this paper will be referenced to 1 μPa in seawater, so we shall drop the additional text.

These terms combine to form the passive sonar equation [10]:

$$SL - TL \geq NL - DI + DT \tag{2.3}$$

The right hand side of Equation (2.3) relates the technical performance of the sonar system in its immediate environment, in this case the acoustic modem receiver on the AUV in seawater. The detection threshold and directivity index, closely tied to signal processing, are immaterial to this thesis and will not be discussed further. The noise level consists of the noise at the receiver, which comes from two parts: first, the self-noise within the receiver itself, and, second, the ambient or background noise at the receiver from biologics, shipping, seismic movements, weather, etc. At the frequency of the WHOI acoustic modem, 23–27 kHz, the background noise is primarily wind-driven with some biologic activities [13]. The source level of the WHOI acoustic modem is a fixed quantity related to the 100W transmission power, which equates to approximately 190 dB [5]. The remaining term, transmission losses, consist of spreading and absorption effects and losses at the boundaries. They will occupy the remainder of this section since they drive the operating range of the acoustic modem and form the core of acoustic ranging methods.

5. Spreading and Absorption

Sound radiates from the acoustic modem in a roughly spherical manner until it interacts with a boundary layer, whether the surface or the bottom. While travelling, each of the rays follows a curvilinear path as previously discussed in Section II.B.3. If, at the point of transmission, we consider the acoustic message to be a sphere with a finite amount of energy, the energy at the wave front decreases proportionally to the increase in the surface area of the sphere, which can be approximated as the square of range (r). The same amount of energy must cover this larger area and thus the intensity weakens. However, if we assume that we are operating in shallow water and that the acoustic transmission will interact with a boundary layer, the spreading becomes cylindrical and reduces the loss rate, in dB, by half, as shown below [10].

$$TL_{Spreading} = 10\log r^2 = 20\log r$$
$$TL_{Cylindrical} = 10\log r \tag{2.4}$$

Absorption results from three separate phenomena: shear viscosity, ionic effects, and pressure (depth). Transmission loss due to absorption is substantially worse in seawater than in pure water due to the ionic equilibria. We need not dive into each phenomenon in detail, but the cumulative effects of absorption at the frequency of interest amount to 5–10 dB per kilometer, assuming a constant pressure (depth) and depending on the temperature and salinity of the seawater [10].

6. Losses at the Boundary Layer

As Figure 4 showed, a sound signal from the acoustic modem can reflect off the surface and bottom multiple times before reaching a receiver. Each of these bounces will incur losses. At the air-ocean interface, nearly all the sound is reflected, vice transmitted through the boundary, so the loss is smaller, though rough surfaces can result in additional losses from scattering. At the ocean bottom, the losses are governed primarily by Snell's Law, including the ray grazing angle (θ), sound speed (c), and the density (ρ) of both the ocean floor and water layer directly above it [14].

$$BL = 20\log_{10}\left|R_{12}\right|^n$$
$$R_{12} = \frac{m\sin\theta_1 - (n^2 - \cos^2\theta_1)^{1/2}}{m\sin\theta_1 + (n^2 - \cos^2\theta_1)^{1/2}} \tag{2.5}$$
$$m = \frac{\rho_2}{\rho_1}, n = \frac{c_1}{c_2}$$

The porosity of the ocean bottom and the grazing angle drive the losses, with additional input from the sedimentary layers, surface roughness, presence of biological materials, air bubbles, and other attenuation effects. Providing a single, shorthand calculation, as we did for cylindrical spreading losses, is not possible. However, Urick [10] reports that bottom losses can range from 0–30 dB per bounce.

C. ACOUSTIC RANGING, ONE WAY TRAVEL TIME

One-way travel time (OWTT) is the most widely accepted model for acoustic ranging in the field today [15]-[19]. This method reduces the complexities presented in the preceding sections into the standard kinematic formula of speed multiplied by time. The advances in the field have largely revolved around the timing aspect of the equation, through characterization of precision clocks, as in [17], and the programmatic and algorithmic details of reducing uncertainty in the actual time of flight (TOF) measurement. Discussions of the sound speed aspect of the equation have remained largely unaddressed, with researchers assuming an isovelocity sound speed profile and, therefore, straight line, vice curvilinear, ray paths. These ranges underestimate the actual range because of the effects of Snell's Law as previously discussed. However, the accuracy is within acceptable margins (<1 m) for the range of interest and the calculations are not computationally expensive to run, so the OWTT framework makes logical sense. Accounting for transmission losses in acoustic ranging explicitly adds several orders of magnitude in difficulty given the variability of the factors to weather, geography, salinity, bottom type, etc., and therefore will not be addressed in the OWTT formula or further in this thesis.

The OWTT equation will be calculated using the standard kinematic formula:

$$Range = V_{sound}(t_{arrival} - t_{transmission}) \tag{2.6}$$

Calculating the time of flight will be accomplished through the timestamps that the WHOI acoustic modem applies to the incoming and outgoing messages. The speed of sound will be calculated from the corrected Del Grosso sound speed equation discussed in Section II.B.2 using measurements from the onboard CTD sensor. In terms of uncertainty calculations, empirical testing of the clocks onboard the REMUS vehicles at NPS indicates no clock drift over eight hours. Similar results from [16], [17], [19], and [20] validate this conclusion. Therefore, we will neglect any uncertainty added from time synchronization issues. For the uncertainty of sound speed, the results from [21] that show the Del Grosso sound speed equation to have an assumed Gaussian distribution with a mean of 0.3 m/s and a standard deviation of 0.05 m/s, assuming perfect sensor

inputs for pressure, temperature, and salinity. To put the uncertainty into physical perspective, two AUVs 500 meters apart would see an acoustic range error of 0.0996 ± 0.0332 meters to two standard deviations (2σ). Integrating this equation into the system model needed for MVSLAM will be done in Section IV.

This section presented the equipment used in this thesis, reviewed sound propagation in an ocean environment, and discussed a simple, widely-used technique for acoustic ranging. We can use the highly uncertain nature of sound propagation to help reduce position uncertainty in an AUV. The implementation of that concept is the focus of both the existing SLAM literature and algorithms, presented next in Section III, and in the proposed use of acoustic communications for navigational accuracy developed later in Section IV.

THIS PAGE INTENTIONALLY LEFT BLANK

III. SIMULTANEOUS LOCALIZATION AND MAPPING

This section builds the case for probabilistic robotics from first principles by examining adaptation of stochastic elements into traditional control system formulations. It will then discuss, in depth, the development of iSAM2, the SLAM algorithm used on the REMUS vehicles at NPS, and will illustrate the performance of the algorithm with a small example. iSAM2 will play a foundational role in the development of a distributed, collaborative SLAM framework in Section IV.

A. INTRODUCTION

1. Position Uncertainty in Robotics

Smith, Self, and Cheeseman [22] first postulated positioning in robotics as a stochastic, rather than deterministic, problem. This fundamental shift in perspective allowed engineers and scientists to incorporate positional uncertainty in the design of the robotic system instead of simply coping with the degradation in quality that could result. The incorporation of probability into this process stems from the realization that no sensor or system is perfect in its sensing or movements, respectively. For example, with the REMUS 100 vehicle, the BlueView forward looking sonar can only sense objects to an accuracy of 0.1 meters in the range direction and 1.2 degrees in the bearing direction. The onboard control system can command the electrical motor to spin the propeller at 2500 RPM, but the known and unknown characteristics of the system may result in the propeller only spinning 2480 RPM, for example. The difference results in slightly less speed, which forces the uncertainty about the vehicle's position to grow. The mathematical representation of a system expanded from the dynamics model to include a system covariance matrix that shows the probabilistic relationship between the state variables.

To ground the work, we discuss the approach to SLAM algorithms from its roots in control systems theory. In Equation (3.0), shown in the canonical discrete state-space form, the first row constitutes the system process or dynamics model, and the second the measurements by the system [23]. These are matrix equations resulting in assumed linear

relationships. The position at the next time step, x_{k+1}, is a function of the dynamical model, such as dead reckoning navigation of an AUV, with additive noise ω_k. Unless explicitly known to be otherwise, all system noise is assumed to be independent and identically distributed (i.i.d.), zero-mean and Gaussian, also known as Gaussian white noise. The measurements of the system, z_k, from acoustic ranging via a beacon, for example, are also subject to Gaussian white noise υ_k. An illustration of this in the context of SLAM will be beneficial.

$$\begin{aligned} x_{k+1} &= \Phi_k x_k + \omega_k \\ z_k &= H_k x_k + \nu_k \end{aligned} \tag{3.0}$$

2. Sources of Uncertainty

The combination and propagation of the process and measurement noise, ω_k and υ_k respectively, results in a probabilistic distribution of the vehicle's position. That distribution is assumed to be Gaussian since all components of the uncertainty terms are Gaussian as well. The vehicle has a calculable probability of being at a given point from the mean position. The same can be applied to the position uncertainty of landmarks. For ease, we define the position uncertainty (PUC) as a Gaussian ellipsoid and it is the graphical estimate of the position uncertainty of the vehicle at a given time. The ellipsoid can be projected onto the horizontal plane, as an ellipse, to show the area that the AUV may be in. We assume that all ellipses represent a 95% probability (two standard deviations) of being inside the ellipse. The PUC size changes over time as the errors compound.

From an inertial navigation-only perspective, the PUC will grow over time as the errors in the INS compound. These errors stems from the engineering tolerances of the gyros and accelerometers in the INS, the ability to precisely sense the position of the inertial measurement units or motion of the accelerometers, and the precision with which the software can extrapolate the estimated position from that noisy data. The inputs into that calculation, such as the commanded vehicle speed, gyrocompass heading, the current

data from the ADCP, etc., all introduce additional errors. The magnitude of the error for a given time step is relatively constant, usually varying with physical parameters, such as current, but over time, those errors are additive. For the Kearfott INS installed on the REMUS, the error can be summarized as approximately 0.5% per distance traveled, as previously stated. In Equation (3.0), these uncertainties manifest in the ω_k term.

Since we will be examining SLAM, which relies on the ability of the vehicle to sense environmental features, the errors within the sensing systems must also be considered. For example, a forward looking sonar mounted on the front of the AUV provides image data up to 5 Hz relative to the AUV's position. A detection and tracking procedure can be used to resolve the relative bearing and range to the vehicle's nose. That procedure will have uncertainty associated with it, manifesting as uncertainty in bearing and range, which can be transformed to the AUV's local coordinate system for incorporation. The errors from the sensing equipment reside in the υ_k term of Equation (3.0). A small example in the next section provides additional insight into this area.

3. SLAM as a Stochastic Process

SLAM, as the name suggests, is the ability to map an area and navigate off of that map in real time. With the implementation of SLAM onto a mobile robot, we can consider the robot conducting two primary evolutions to accomplish this: sensing the environment and movement within that environment. In some robotic applications, the robot must stop to sense, while in others, such as underwater, the vehicle is continually in motion while sensing, to include hovering or station-keeping. However, the discretization of the latter case removes the complications associated with that motion.

Using the REMUS vehicle as an example, we can see how these probabilistic relationships function in a SLAM environment. The REMUS vehicle uses a twelve variable state vector, or pose (**x**), in Equation (3.1) that provides six degrees of freedom in movement since it contains both linear (x,y,z) and angular (ϕ,θ,ψ) position and rates (u,v,w for linear, and p,q,r for angular). The associated covariance matrix, or relationship

between each of the state variables, is, by definition, a 12x12 matrix. Or more generally, an n-dimensional state vector will have an n-by-n covariance matrix, $\Sigma(x)$.

$$x = \begin{bmatrix} x \\ y \\ z \\ u \\ v \\ w \\ \phi \\ \theta \\ \psi \\ p \\ q \\ r \end{bmatrix} \qquad \Sigma(x) = \begin{bmatrix} \sigma_x^2 & & & & & & & & & & & \\ & \sigma_y^2 & & & & & & & & & & \\ & & \sigma_z^2 & & & & & & & & & \\ & & & \sigma_u^2 & & & & & & & & \\ & & & & \sigma_v^2 & & & & & & & \\ & & & & & \sigma_w^2 & & & & & & \\ & & & & & & \sigma_\phi^2 & & & & & \\ & & & & & & & \sigma_\theta^2 & & & & \\ & & & & & & & & \sigma_\psi^2 & & & \\ & & & & & & & & & \sigma_p^2 & & \\ & & & & & & & & & & \sigma_q^2 & \\ & & & & & & & & & & & \sigma_r^2 \end{bmatrix} \tag{3.1}$$

The off diagonal terms in the covariance matrix represent the cross-correlation between the individual state variables.

The robot begins by sensing a landmark from its current position. At this point, the robot has defined a PUC, as indicated by the red circle in Figure 5.

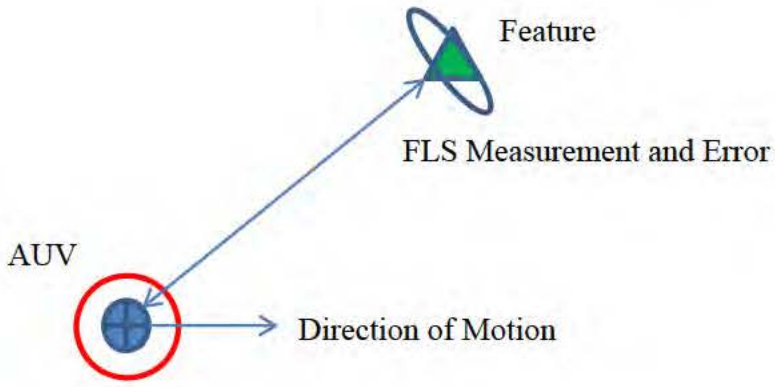

Figure 5. The robot, with a finite PUC, senses a landmark and takes a sensor measurement. The uncertainty of the feature and the AUV are the blue ellipse and red circle, respectively.

The sensor measurement of the landmark will have uncertainty associated with it, as previously stated. In the simplest sense, the error from the measurement of the landmark can be superposed onto the vehicle and combined with the vehicle's current PUC through a Bayesian inference to produce a new PUC. The mathematical implementation of the Bayesian inference will be covered in Section IV.C.1. The vehicle then moves and takes another measurement of the same landmark, shown in Figure 6.

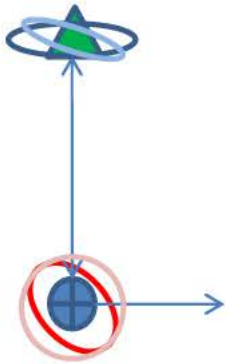

Figure 6. The robot, with an updated PUC, has moved a fixed distance and takes a measurement of the same landmark. The initial PUC is in light red for comparison.

The incorporation of the sensor measurement is again superposed onto the vehicle and algorithmically combined to form a new PUC measurement. In Figure 7, we see the result after the second time step.

Figure 7. After two measurements of the same landmark, the robot's PUC, the red ellipse is substantially smaller than it was at the beginning. The initial ellipse is in light red to show the reduction. The updated uncertainty of the feature is shown as the light blue ellipse, and is markedly smaller than the initial, shown in dark blue.

We can see visually that using sensor measurements of environmental features allowed us to reduce the AUV's PUC significantly. Simultaneously, all measurements of the feature are integrated through a Bayesian inference or other statistical methods. The resulting positional uncertainty of the AUV and the feature is smaller than if only a single measurement had been taken. The end result of the SLAM process is that the AUV has constrained its navigational uncertainty, which improves map accuracy, while creating a map of the environment.

This simple example showed the basic process for SLAM. The effects on each of the twelve individual state variables may or may not be related to the SLAM process, depending on the information obtained with the measurements. In most implementations in the underwater environment, the SLAM process only affects linear position in the horizontal plane (x, y) and heading (ψ). The rest of the state variables are generally a function of the vehicle control systems and physical system design. For notational convenience, they will be omitted going forward in this thesis.

This example also highlights the challenges associated with SLAM. While not discussed in the context of the example, several other algorithms are vitally important for

SLAM operations. First, the detection and tracking of features is not an exact science, as discussed in Section III.A.2. Increasing the performance of that algorithm will improve navigational and map accuracy. Second, this example assumed the ability to unambiguously differentiate between features. Only one feature was presented in this example, but features may appear close together and associating measurements with the correct feature is crucial to ensuring stable algorithm performance and maintaining map accuracy. This process of correlating measurements with features is known as data association. Lastly, the ability to return to a previously detected feature and recognize it as previously detected is known as loop closure. Loop closure is a vital aspect of making SLAM algorithms with operational utility.

4. Optimal Estimation

Rudolf Kalman's [24] seminal paper in 1960 proving the optimality of his new linear filter opened a new field known as optimal estimation, in which we attempt to estimate uncertain processes such as AUV motion. Kalman filters assume the system is linear and the noise is Gaussian i.i.d and optimally balance the dynamic uncertainty inherent in process and measurement models. The linear Kalman filter has spun off into several new fields of filtering: particle filters, extended Kalman filters (EKF), which considers non-linear motion, extended information filters, and smoothing filters, to name a few of the major ones. Most robotic systems use an EKF, or a variant thereof, in SLAM for computational efficiency. But some, such as the filter implemented on the NPS REMUS vehicles, use a smoothing filter.

EKFs consider the information at a given time step, with all previous information summarized in the prior state estimate. The EKF incorporates any sensor measurements and linearizes the equations of motion at the current time step to produce a updated estimate of the robot pose. Smoothing filters, on the other hand, consider all prior information at each time step without summarizing. While they have historically been too computationally inefficient for most real time applications, faster smoothing filters have emerged concurrently with processing power and hardware advances, iSAM2 being one of them. Using iSAM2 provides a more accurate estimate than a traditional EKF-based

SLAM approach since it revisits all previous estimates of features and navigation estimates at each time step, which is highly desirable in the underwater environment.

C. INCREMENTAL SMOOTHING AND MAPPING

1. Process and Measurement Models

Developed by Kaess and Dellaert [3], [25], iSAM2 fulfills the core goals of any SLAM process: exactness and computational efficiency. An EKF, essentially a non-linear Kalman Filter, linearizes about a point at a given time step, which is then incorporated into the prior state estimate, unable to be changed in the future. iSAM2 provides for fluid variable relinearization, which seems complex, but is very efficient since in SLAM applications, the information matrix underlying the feature map that we are trying to linearize about is at all times sparse [25].[2]

A SLAM process is affected by both the executed vehicle trajectory and a map of the features, which as previously stated, are both uncertain. Kaess starts with the assumption of a non-linear model and converts this into a least squares problem, which allows us to estimate all unknowns given the available measurements through a *maximum a priori* (MAP) estimate. We begin by stating that SLAM follows a basic process and measurement model, akin to the state-space model provided in Equation (3.0):

$$\begin{aligned} x &= Ax + Bu + \omega \\ z &= Hz + \upsilon \end{aligned} \tag{3.2}$$

ω and υ are the zero-mean, i.i.d. Gaussian noise associated with process and measurements, respectively. In this case, the A and B matrices, the equations concerning dynamics and control inputs, can be collapsed into a single function that describes the dynamic motion of the vehicle—the process model. The measurement equations can be similarly adjusted to account for the measurement of landmarks and the subsequent data association. Equation (3.2) thus reduces as shown below:

$$\begin{aligned} x &= f(x,u) + \omega \\ z &= h(x,l) + \upsilon \end{aligned} \tag{3.3}$$

[2] All information and equations in this section, for subsections 1-5, are from [25] unless explicitly cited otherwise.

l is the landmark that has been sensed and factors into the measurement model, z, of Equation (3.2). The explicit time dependencies of the system have been omitted for simplicity, known as discretization, but these equations do vary with time, and multiple landmarks can exist.

2. Linearization

The construction of the MAP estimate through least squares requires the linearization of both the process and measurement models around the current estimates. We accomplish this through a Taylor series expansion of the two equations in Equation (3.3), which yields the resulting three Jacobian matrices.

$$\begin{aligned} F &= \left.\frac{\partial f(x,u)}{\partial x}\right|_{x_t,l_t} \\ H &= \left.\frac{\partial h(x,l)}{\partial x}\right|_{x_t,l_t} \\ J &= \left.\frac{\partial h(x,l)}{\partial l}\right|_{x_t,l_t} \end{aligned} \tag{3.4}$$

These matrices are collected into a larger matrix A along with a fourth special matrix, G, that allows us to not consider the dx/dx terms. These matrices are oriented in the A matrix as follows:

$$A = \begin{bmatrix} G & 0 & 0 & 0 \\ F & H & 0 & 0 \\ 0 & F & H & 0 \\ 0 & J & 0 & J \end{bmatrix} \tag{3.4}$$

The least squares process can be qualitatively described as seeking the minimum of a given argument consisting of squared terms. In this case, the four Jacobian matrices and the navigation (process) and measurement prediction error terms, a and c, respectively, can be arranged to represent the least squares estimation problem:

$$\delta\theta^* = \arg\min_{\delta\theta}\left\{\sum_{i=1}^{M}\left\|F_i^{i-1}\delta x_{i-1} + G_i^i \delta x_i - a_i\right\|_{\Lambda_i}^2 + \sum_{k=1}^{K}\left\|H_k^{i_k}\delta x_{i_k} + J_k^{jk}\delta l_{jk} - c_k\right\|_{\Gamma_k}^2\right\} \tag{3.5}$$

After some algebraic manipulation, it can be proven that Equation (3.5) reduces as follows:

$$\theta^* = \arg\min_{\theta} \|A\theta - b\|^2 \tag{3.6}$$

Equation (3.6) is now in the standard form for linear least squares (LLS) estimation, where θ is the concatenation of the vehicle pose and the landmark variables and b is the concatenation of the navigation prediction and measurement prediction errors. θ^* becomes the new prediction. This LLS problem can be solved using standard methods, such as QR factorization or Cholesky decomposition. Kaess opts for QR factorization since it paves the way for computationally easier incremental updates to the *A* matrix, which grows over time. The unique solution to the LLS problem is also termed, in this application, the square root information matrix (SQIM). iSAM2 updates the SQIM as new information becomes available. It gains efficiency by using the previous solution and only performing the calculations on the new measurements.

3. Variable Reordering

Variable reordering is a linear algebra technique that reorders the columns of the information matrix. Kaess applies it in blocks, each of which conforms to a single pose node or landmark [3]. This method reduces the duplication of landmarks if the robot revisits a previously sensed landmark, or closes the loop in community standard language. Failing to recognize loop closure events in SLAM problems leads to duplication of previously visited landmarks, and, for iSAM2 in particular, the appearance of non-zero entries in the R matrix following QR factorization—a highly undesirable result. Kaess solves this problem through the application of a common linear algebra technique, column approximate minimum degree (COLAMD), to blocks in the R matrix that correlate to previous AUV positions and landmark positions.

4. Process Results

The process described in the preceding sections is conducted each time the AUV senses a new landmark. Additional measurements of the same landmark only provide

amplifying information for an existing entry in the A matrix and thus are not added. The detection of a new landmark creates a new set of entries for the LLS process: 1) the position of the landmark, 2) the constraint, or line, between the AUV position and the landmark, and 3) the vehicle position at the time of the first measurement. The latter entry is defined as a pose node in community standard language. The LLS process solves the entire SLAM problem, consisting of all pose nodes and landmark entries since the mission began. This adds the benefit of being able to linearize at each pose node instead of trying to choose a single linearization point for all previous data as an EKF would.

5. Mathematical Example

To provide additional insight into the inner workings of the iSAM2 algorithm, consider the simplified example provided in Section III.A.3, revised slightly for clarity. The evolution of the iSAM2 computations will be shown over the time step to show each process individually. We begin by applying a coordinate frame to Figure 8, with the AUV starting at the origin, with a forward velocity of $u = 1\,\text{m/s}$, no side slip velocity, and heading 090°, along the x-axis. For simplicity, we have set the time increment, dt, at 25 seconds.

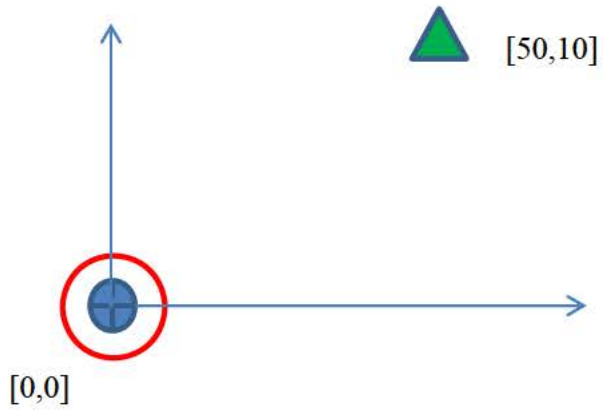

Figure 8. The example problem from Section III.A.3 now with a coordinate system overlaid.

After the first time step, the AUV is now at (25,0) and has detected the feature, shown in Figure 9. The sonar system identifies the feature and passes the information to iSAM2, which runs an algorithm called Joint Compatibility Branch and Bound for data association to produce an estimate of the feature's position [26]. If the feature has not been previously detected, iSAM2 adds the feature to its feature database and stores the information. Subsequent sensor measurements of the feature reduce the position uncertainty of both the feature and vehicle.

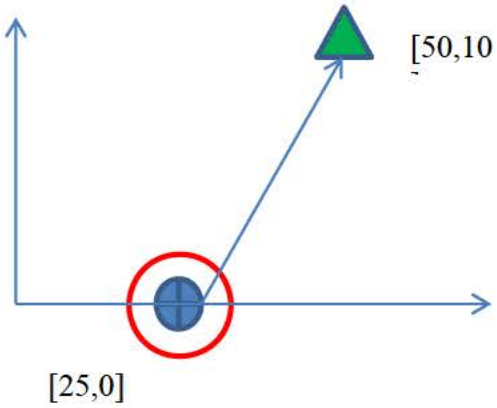

Figure 9. AUV position after one 25-second time step. The AUV has detected the feature at [50,10] and made the pose to landmark constraint in iSAM2.

iSAM2 solves the non-linear LLS problem to produce the estimate of both the AUV's trajectory, inclusive of all pose nodes, and all features detected. Graphically, this can be represented through a visual sparsity pattern plot, or spy plot, which shows which elements of a matrix have non-zero entries. In this example, we show the A and R matrices to show how QR factorization supports fluid variable reordering. Figure 10 shows the spy plot for the A matrix with the two calculated pose nodes and measurements of the single landmark. Figure 11 shows the R matrix following QR factorization of the A matrix.

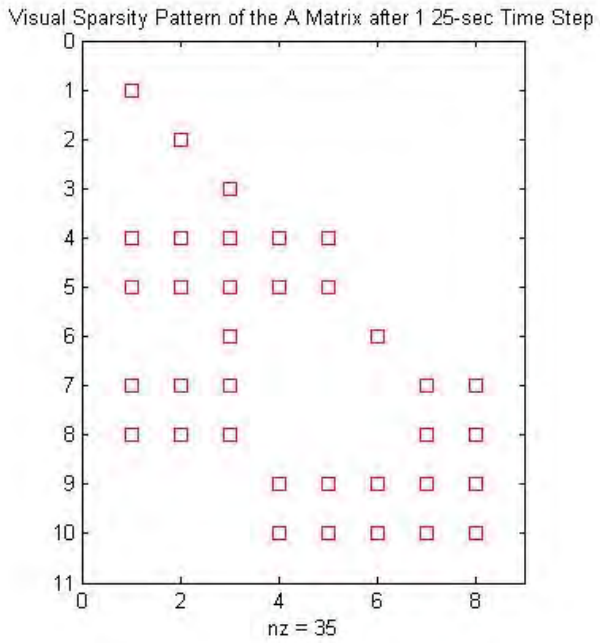

Figure 10. The visual sparsity pattern of the A matrix after a single 25-second time step with one feature detected.

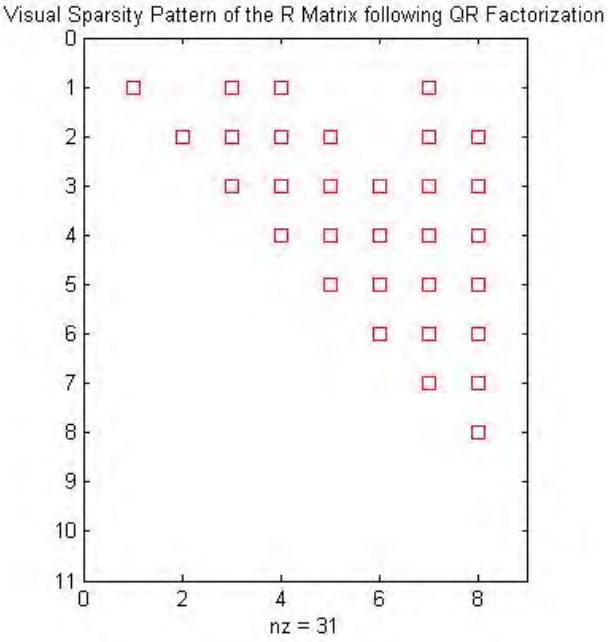

Figure 11. The visual sparsity pattern of the R matrix following QR factorization of the A matrix. Some of the entries may have changed during QR factorization as a result of applying Givens rotations to specific entries in the lower half of the A matrix.

The addition of a new measurement yields faster results when using incremental updating. Instead, as previously stated, of factoring the entire A matrix gain, the new measurement is simply added to the bottom of the R matrix and Givens rotations applied to make the new matrix, R^*, upper triangular again. In this example, that savings in computational efficiency would not be noticed, but in larger data sets, this approach yields significantly faster results.

Unlike the qualitative example provided at the beginning of this section, recovering the uncertainty values to display them as an ellipse is not straightforward. Unlike an EKF, where the covariance matrix is clearly identifiable throughout the process, the uncertainty information is more hidden in iSAM2. In a small case such as this, we can recover the covariance information through from Equation (3.7). However, once the R matrix becomes large, this equation becomes computationally burdensome and a different method must be used [27].

$$P = \left(R^T R\right)^{-1} \tag{3.7}$$

In this example, Equation (3.7) produces an 8x8 matrix with the following values. These show the covariance information associated with the vehicle pose estimates and the detected landmark. It should be noted that after one time step, the uncertainty here is still rather small and should not be viewed as typical, especially for underwater problems where.

$$P = \begin{bmatrix} 0.01 & 0 & 0 & 0.01 & 0 & 0 & 0.01 & 0 \\ 0 & 0.01 & 0 & 0 & 0.01 & 0 & 0 & 0.01 \\ 0 & 0 & 0.01 & -0.25 & 0 & 0.01 & -0.5 & 0.1 \\ 0.01 & 0 & -0.25 & 6.2695 & -0.0011 & -0.2497 & 12.5105 & -2.4989 \\ 0 & 0.01 & 0 & -0.0011 & 0.0171 & 0 & 0.0011 & 0.0129 \\ 0 & 0 & 0.01 & -0.2497 & 0 & 0.01 & -0.5003 & 0.1001 \\ 0.01 & 0 & -0.5 & 12.5105 & 0.0011 & -0.5003 & 25.0195 & -5.0011 \\ 0 & 0.01 & 0.1 & -2.4989 & 0.0129 & 0.1001 & -5.0011 & 1.0171 \end{bmatrix} \tag{3.8}$$

While equation (3.8) looks cluttered, we are only concerned with, for this example, with the values in elements [1, 1] and [2, 2], which represent the position

uncertainty of the AUV in both x and y. The position uncertainty of the landmark is in the lower right quadrant. This information is highly valuable from a mapping perspective.

This chapter discussed the algorithmic applications of managing the stochastic nature of robotics. It took a close look at the iSAM2 algorithm developed by Kaess and Dellaert [3], [25] and illustrated the algorithm with a simple example. NPS uses iSAM2 onboard the REMUS AUVs for research work and the algorithm will be the primary platform for integrating information from acoustic communications for collaborative SLAM.

THIS PAGE INTENTIONALLY LEFT BLANK

IV. COLLABORATIVE MULTIPLE AUV SLAM

A. RECENT WORK

We begin the development of an MVSLAM algorithm with a review of the recent literature focused on this area. The existing body of work can be loosely partitioned into five separate areas: centralization and hierarchy, beacon-aiding, cooperative SLAM, and dynamic SLAM.

1. Centralization and Hierarchy

Early approaches to the MVSLAM problem focused on creating a centralized solution onboard a single vehicle, as in [28], or a joint map between all vehicles with common nodes that facilitates cooperative loop closure, as in [29]. Moratuwage, Vo, and Wang [30] focus on the creation and communication of individual submaps, which can then be used by other vehicles for measurements or additional data association. Finally, Moratuwage et al. [31] proposes a single EKF SLAM algorithm for multiple vehicles.

Alternate approaches began to emerge as researchers postulated highly decentralized MVSLAM solutions, which facilitated more efficient use of processing power and allowed each vehicle to maintain estimates of the whole group. These researchers began to embrace the difficulty of having all robots communicate with all other robots at each of the prescribed times. Leung, Barfoot, and Liu [32] propose a framework that creates a centralized-equivalent solution in a sparsely-communicating and dynamic environment. Nerurkar and Roumeliotis [33] explore creating centralized-equivalent estimates in an asynchronous network. Bahr, Walter, and Leonard [34] explored the possibility of an individual vehicle utilizing a bank of filters to track measurements and cooperatively localize other vehicles through trilateration. Hua et al. [35] present a communications-heavy approach in which all robots share their local sensor data. All receiving robots can then process all information and arrive at the same estimates, increasing robustness to individual failures. Most recently, Walls and Eustice [36] reframe the problem in terms of client-server relationships and transmit poses to allow all client vehicles to reproduce central estimates, explicitly developed for highly

bandwidth-limited underwater communications. However, the authors note that their method does not solve for loop closure, making the approach impractical for our purposes.

2. Beacon-Aided SLAM

A classic approach to reducing position uncertainty, beacon systems can be either mobile or static and rely on precise position information which is supplied to robots through queries or constant communications. Ultra-short baseline (USBL) systems are very common implementations of beacon-aided navigation. This focuses on beacon-aiding for SLAM operations and is most closely related to the work in this thesis in terms of algorithmic implementation of acoustic communications. Erol et al. [37] offers an approach whereby mobile sensors periodically ascend to the surface for a GPS fix and communicate their exact position upon descent to the other nodes in the network, which localizes all sensors in a multi-stage algorithm. Bahr, Leonard, and Fallon [38] provide another very similar approach; however, the communication between vehicles and the follow-on algorithm serve primarily for trajectory selection vice reducing position uncertainty. Bahr, Leonard, and Martinoli [39] present another very similar approach that seeks to use one vehicle as a dedicated beacon vehicle, surfacing at proscribed intervals and transmitting its position information to the rest of the network. Intra-vehicle range estimates complete the picture. This approach is the most related to the work of this thesis, but is not appropriate based on the required frequency of surfacing and acoustic communications being counter to the principles of tactical security.

3. Behaviors and Cooperative SLAM

This emerging branch of MVSLAM focuses on maximizing certain information or other parameters through vehicle orientations, trajectories, or even path planning. Stipes et al. [40] offers an approach to MVSLAM that utilizes distributed control algorithms to adapt individual robot behaviors in real time to maximize SLAM yields and improve robustness. Pham and Juang [41] propose an algorithm that disperses robots intelligently to achieve a prescribed minimum SLAM accuracy as well as adaptively

balance the needs of both localization and exploration in a communications-limited environment.

4. Dynamic Features in SLAM

Perhaps the most recent branch of SLAM research, dynamic problems refer to the alteration of maps over time, such as in warehouse inventory problems, or the tracking of moving targets. Traditional SLAM architectures only work with static features. Movement of landmarks would severely degrade system performance and potentially cause the operative SLAM algorithm to collapse. Lee, Clark, and Salvi [42] present a first-generation algorithm that can estimate both static and dynamic features in addition to the vehicle pose. They accomplish this through the use of probability hypothesis density filters and relate all features to the vehicle location at each time step. Abrate et al. [43] provides an approach that bridges traditional SLAM with the environments envisioned in [42] through the use of a map updating technique with the aim of long term mapping operations in the same physical location.

B. PROPOSED APPROACH

The current approaches to MVSLAM in the literature all rely on frequent communications between robots to alter behaviors, estimate the full state of a group of robots, or transmit precise positioning information from a position source such as GPS. While our proposed approach will be most closely related to beacon-aided SLAM operations, these approaches in the present body of SLAM literature are not appropriate for this work because of our explicit consideration of tactical security. We instead focus on minimum acceptable performance, not perfect or optimal performance, in order to minimize acoustic communications and vehicle surfacing, thus maximizing tactical security. Thus, if the individual SLAM solution is acceptable, the AUV will not communicate. This heuristically-evaluated cost function will rely on inferential solutions using Bayesian methods. Additionally, unlike many of the algorithms presented in the previous section, we do not require the compilation of a global feature map on all vehicles. We instead leave the construction of the global map to post processing, where planners can then decide how best to navigate through or neutralize the minefield.

The remainder of this section will proceed as follows. First, we will derive and demonstrate the principles and utility of a Bayesian inference. Second, we will discuss the value that acoustic communications can add in reducing position uncertainty. Finally, we will qualitatively describe and develop the algorithm that will produce updated covariance estimates and show that using acoustic communications as an additional measurement provides significant added value. Finally, we will discuss the performance metrics that will be needed to evaluate system performance. Simulation results and the analysis of algorithm performance will be reserved for Chapter V.

C. INFERRING COVARIANCE

In this section we discuss the application of a Bayesian inference as a way to reduce position uncertainty for *n*-number of AUVs. This section will present the relevant equations with supporting examples and provide first-order insight into the value of acoustic communications and ranging to uncertainty reduction, as well as explore the major factors that we must consider when using inferential methods.

1. The Bayesian Inference

Bayesian inferences use Bayes' Theorem to update a probability estimate for a state as additional measurements are taken. Equation (4.1) shows Bayes' Theorem, read as the probability of B given A is equal to the probability of A given B multiplied by the probability of A occurring all divided by the probability of B occurring. A and B can be any event that can be described by a probability density function.

$$P(B \mid A) = \frac{P(A \mid B)P(A)}{P(B)} \tag{4.1}$$

For the purposes of robotic mapping, we assume that our sensors have noise that can be approximated as a Gaussian or normal distribution about a given mean, μ, usually zero, with a specified covariance, σ^2. The position uncertainty for an autonomous vehicle is initially assumed to be a Gaussian spheroid, which will iteratively change into a Gaussian ellipsoid as additional measurements of the surrounding environment are taken assuming linear dynamic and measurement models. The standard formula for a Gaussian distribution is as follows:

$$y = f(x \mid \mu, \sigma) = \frac{1}{\sqrt{2\pi\sigma^2}} e^{-\frac{1}{2}\left(\frac{x-\mu}{\sigma}\right)^2} \tag{4.2}$$

Qualitatively, a Bayesian inference makes an assumption about the likelihood of a given measurement being accurate through the use of a weighting formula that is then multiplied by the prior state. The following equations are evaluated using a two-dimensional example, which closely approximates the problem at hand.

$$P(\theta \mid y) = \frac{P(y \mid \theta)P(\theta)}{P(y)} \propto cP(y \mid \theta)P(\theta) \tag{4.3}$$

θ is the set of parameters that define the Gaussian distribution and y is the measurement. The constant, *c*, is a normalization constant. Since we cannot measure the position of the AUV directly to estimate the updated state, we are instead interested primarily in the inferred covariance term, which we can feed back into the host AUV's iSAM2 algorithm to reduce the closed loop position uncertainty. For clarity, the variance of the updated distribution, denoted as the covariance at time *k+1* given the covariance matrices at time *k*, is expressed as a function of *n*-number of input covariance matrices:

$$\Sigma_{k+1|k+1} = \left(\frac{I_{2x2}}{\Sigma_1} + \frac{I_{2x2}}{\Sigma_2} + \cdots + \frac{I_{2x2}}{\Sigma_n} \right)^{-1} = \begin{bmatrix} \sigma_{xx}^2 & \sigma_{xy}^2 \\ \sigma_{yx}^2 & \sigma_{yy}^2 \end{bmatrix} \tag{4.4}$$

a. A Numerical Example

Consider a two-dimensional problem, akin to AUV localization problems, with two AUVs. Their positions are not relevant to the example, but they have the following covariance information at time *k*:

$$\begin{aligned} \Sigma_k^1 &= \begin{bmatrix} 20 & 5 \\ 5 & 20 \end{bmatrix} \\ \Sigma_k^2 &= \begin{bmatrix} 10 & 1 \\ 1 & 10 \end{bmatrix} \end{aligned} \tag{4.5}$$

In this case, the first AUV has greater positional uncertainty than the second AUV, and would benefit from the second's better localization. The first AUV needs to

reduce its positional uncertainty and has an acoustic communications link with the second AUV. The second AUV shares its covariance information at time *k* with the first. Ignoring, for the moment, the uncertain effects of acoustic communications, we can calculate the inferred covariance at *k+1* using equation (4.4) and see how the application of a measurement reduces the value of the covariance matrix. Using Equation (4.4), we find:

$$\Sigma^{1}_{k+1|k} = \left[\frac{I_{2x2}}{\begin{bmatrix} 20 & 5 \\ 5 & 20 \end{bmatrix}} + \frac{I_{2x2}}{\begin{bmatrix} 10 & 1 \\ 1 & 10 \end{bmatrix}} \right]^{-1}$$
$$\Sigma^{1}_{k+1|k} = \begin{bmatrix} 6.6319 & 1.0069 \\ 1.0069 & 6.6319 \end{bmatrix} \tag{4.6}$$

These numbers signify the uncertainty in the x- and y-directions as well as the cross-correlation between them. The result in Equation (4.6) reveals a crucial point. The updated result is smaller than the two prior covariance matrices, which means that *any* measurement, regardless of the precision or presence of noise, will reduce the updated uncertainty.

To further emphasize the utility of the Bayesian inference, we can think of the covariance in a visual manner. In a Gaussian distribution, the variance represents the expected value of the squared deviation from the mean. The square root of the variance, the standard deviation, can be viewed as a confidence interval—the probability that the true value lies within those bounds. One standard deviation on either side of the mean equates to a 68.2% confidence interval, two equate to 95.4%, and three to 99.7%. For the position uncertainty of an AUV, we choose a 95% confidence interval (2σ) to govern the size of the ellipse, meaning that the AUV has a 95% probability of being somewhere inside that ellipse at the given moment in time. Constructing the ellipse requires radius values for both the semi-major and semi-minor axes as well as the rotation angle from a standard Cartesian coordinate system. From Equation (4.4), the semi-major and semi-minor axes are the square root of the entries on the main diagonal. We find the rotation angle as follows [44]:

$$\theta' = \frac{1}{2}\tan^{-1}\left(\frac{2\sigma_{xy}}{\sigma_{xx}^2 - \sigma_{yy}^2}\right) \tag{4.7}$$

Thus, from Equations (4.4) and (4.7) we can visually represent the position uncertainty for our example problem in terms of 95% confidence ellipses, as shown in Figure 12.

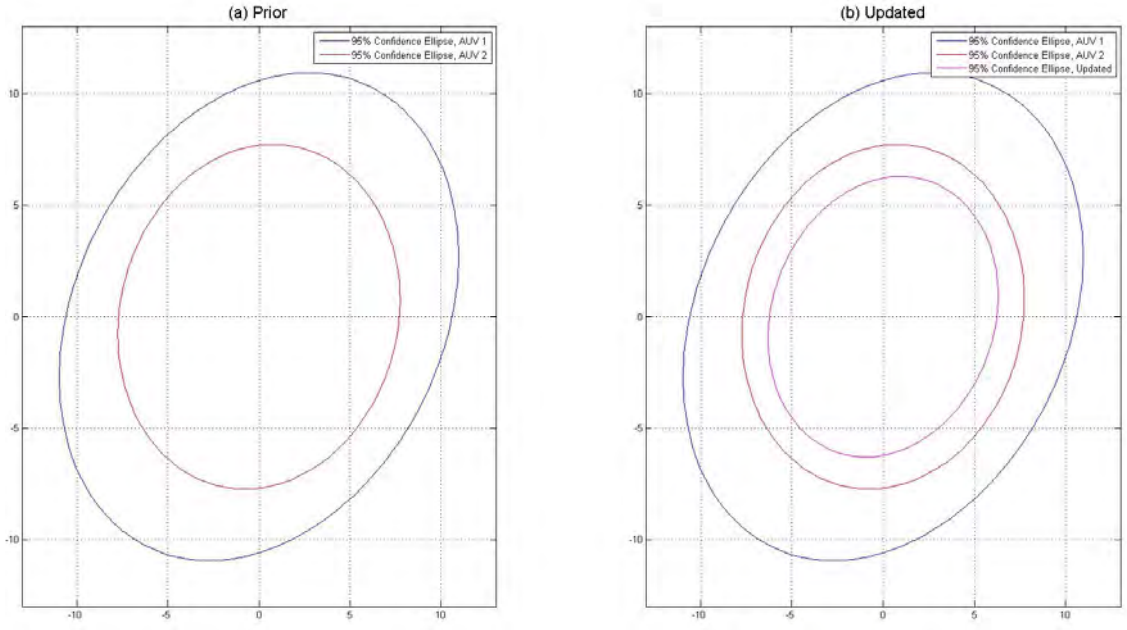

Figure 12. *A priori* 95% confidence ellipses for two AUVs centered at the origin in (a) and after the mathematical integration of the two through a Bayesian inference in (b) with the updated 95% ellipse shown in magenta.

Figure 12 shows the benefit of this mathematical technique in terms of reducing the position uncertainty of an AUV. This example included two AUVs with covariance matrices aligned in generally the same manner. Altering the geometry to place these two ellipses perpendicular to each other will produce a much small updated ellipse, as we will see in the next section.

2. Value of Acoustic Communications and Ranging

This section will discuss the value of acoustic communications and ranging from the aspect of reducing position uncertainty. From the acoustic transmission we can gain

two independent measurements, with associated uncertainties, to reduce the position uncertainty of an AUV. These measurements constitute the creation of a temporary feature within the SLAM framework. First, the acoustic message contains the sending AUV's state information, which includes position, heading, and position uncertainty (covariance). Second, the acoustic transmission, regardless of message content, has a known time of flight, which we can use to calculate range, as discussed previously in Section II.C. While the WHOI micromodem does not have the ability to discern bearing from incoming messages, we can make a few well-founded assumptions about the nature of acoustic communications to exploit the additional measurement from acoustic transmissions.

For short-range navigation and tracking applications, many different industries use an ultra-short baseline system, which consists of a transceiver and transponders that track vehicles using acoustic transmissions. Most commercial USBL systems are accurate to within 0.2% for a slant range from the transponder to the AUV and within 0.1 degrees in bearing, out to several kilometers. That bearing accuracy, already obtainable in multiple commercial systems, will be the core assumption needed to extract the acoustic transmission measurement. We will make similar assumptions with respect to using the acoustic modem in creating a temporary feature.

From the acoustic message we can ascertain the bearing of the acoustic transmission by finding the range and relative bearing between the two AUVs. Using the calculated TOF and error from the DelGrosso sound speed equation, we can determine the error in range as follows, where *rand* indicates a randomly selected value from a Gaussian distribution to account for the uncertainty.

$$\begin{aligned} \sigma_{range} &= \left(\mu_{ss} + \sigma_{ss} \cdot rand\right) \cdot TOF \\ \sigma_{range} &= \left(0.3 + 0.05 \cdot rand\right) \cdot TOF \end{aligned} \tag{4.8}$$

Assuming a bearing accuracy of 0.1 degrees, we can finish constructing the covariance matrix to characterize the uncertainty of an acoustic transmission:

$$\Sigma_{acomms} = \begin{bmatrix} \sigma^2_{range} & 0 \\ 0 & \sigma^2_{bearing} \end{bmatrix} = \begin{bmatrix} (0.3 + 0.05 \cdot rand) \cdot TOF^2 & 0 \\ 0 & 0.1^2 \end{bmatrix} \tag{4.9}$$

a. Numerical Example Revisited

Returning to the example from the previous section, we can show the effect of incorporating this second measurement. Using a baseline sound speed of 1506.16 m/s, we add a measure of Gaussian uncertainty from the parenthetical expression in Equation (4.8) , 0.343 m/s, for a final sound speed of 1506.503 m/s.[3] If we assume the two AUVs are 1000 meters apart and bear 45° relative to each other, we calculate a TOF for the acoustic transmission of 0.6637 seconds. We apply the sound speed uncertainty and TOF to equation (4.9) to produce a covariance matrix for the acoustic measurement, in polar notation:

$$\Sigma_{acomms} = \begin{bmatrix} 0.1511 & 0 \\ 0 & 0.01 \end{bmatrix} \tag{4.10}$$

We now apply Equation (4.4) for the three matrices, the two from the previous section and the acoustic covariance matrix just derived, after rotating by the relative bearing, matrix *R*, to find the covariance at time *k+1*. Since acoustic communications adds additional information to the measurement (the position of the second AUV), the acoustic communications covariance matrix will add to the second matrix, as shown in Equation (4.11). Equation (4.12) shows the numerical example recalculated with acoustic communications.

$$\Sigma_{k+1|k+1} = \left(\frac{I_{2x2}}{\Sigma_1} + \left(\frac{I_{2x2}}{\Sigma_2 + R\Sigma_{acomms}} \right) \right)^{-1} \tag{4.11}$$

[3] This value was obtained by calculating equation (2.1) with the following inputs: T = 15 °C, S = 34 ppt, and P = 400 kg/cm^3.

$$\Sigma_{k+1|k} = \left[\frac{I_{2x2}}{\begin{bmatrix} 20 & 5 \\ 5 & 20 \end{bmatrix}} + \left(\frac{I_{2x2}}{\begin{bmatrix} 10 & 1 \\ 1 & 10 \end{bmatrix} + \begin{bmatrix} 0.707 & -0.707 \\ 0.707 & 0.707 \end{bmatrix} \begin{bmatrix} 0.1511 & 0 \\ 0 & 0.01 \end{bmatrix}} \right) \right]^{-1} \tag{4.12}$$

$$\Sigma_{k+1|k} = \begin{bmatrix} 6.697 & 1.011 \\ 1.011 & 6.636 \end{bmatrix}$$

To better understand the magnitude of reduction provided by the acoustic transmission, we introduce the Frobenius norm, which provides a scalar value of the covariance matrix through a root-sum-square approach, and thus will show the effect of noise or additional measurements more easily.

$$\|A\| = \sqrt{trace(A^T A)} \tag{4.13}$$

Applying this equation to the results obtained in equations (4.6) and (4.12), we see similarities more clearly.

$$\begin{aligned} \|\Sigma_{k+1}\| &= 9.4864 \\ \|\Sigma_{k+1}^{acomms}\| &= 9.5362 \end{aligned} \tag{4.14}$$

Equation (4.14) clearly shows that acoustic communications do not significantly alter the uncertainty information and can thus be used to create temporary features in a SLAM framework. The example problem used in this section is somewhat contrived in that the positional uncertainties of AUVs using SLAM algorithms will likely not be that large, and the governing assumptions of the acoustic transmission must be tended carefully. The values were chosen to make the results of a Bayesian inference explicitly clear.

b. Determining Relative Performance

The reduction in position uncertainty with the application of acoustic communications with USBL-based assumptions is predicated on how USBL systems are physically implemented. The USBL transceiver is usually mounted on a stable surface craft with access to a precise positioning system, such as GPS with an onboard INS. The

accurate transceiver position is what allows the relative accuracy of USBL solution. In this case, the simulated USBL system is mounted on an AUV with not-insignificant position uncertainty, meaning that the correlation of the acoustic measurements to highly accurate position estimates can no longer be assumed. However, an AUV does provide a stable platform from which to conduct acoustic communications and ranging operations.

The stability of the platform allows us to consider the relative performance between vehicles as a criterion for transmitting acoustic messages. We formalize this arrangement with application of Kullback-Leibler divergence, a concept in information theory that calculates the relative entropy gain between two probability density functions to indicate the relative value of the two systems. Kullback-Leibler divergence can be expressed as shown in Equation (4.15).

$$KL \cong \frac{p(x)}{q(x)} \tag{4.15}$$

We adapt the Kullback-Leiber concept of relating probability density functions examine the relative performance between two vehicles. Equation (4.16) shows the relationship between two AUVs at time *k*. We reduce the covariance matrix into a unitary value by taking the sum of the elements on the main diagonal, or the trace.

$$KL \cong \frac{trace(\Sigma_k^1)}{trace(\Sigma_k^1)} \tag{4.16}$$

Equation (4.16) does not have an explicit temporal component, but it is time varying since the covariance matrices in both the numerator and denominator both vary with time as the vehicles navigate and detect features.

c. Aspect Dependence

The example used thus far included covariance matrices for the two AUVs that were nearly collinear, as can be seen visually in Figure 12 with the semi-major and semi-minor axes of each ellipse being approximately aligned. The results obtained were unique to the geometry of this simple problem. Consider the relative difference between the

principle axis angles, which we can use to determine the degree of orthogonality, $\Delta\theta$, derived from equation (4.7) and shown in equation (4.17):

$$\Delta\theta = \theta_2 - \theta_1 = \left[\frac{1}{2}\tan^{-1}\left(\frac{2\sigma_{xy}}{\sigma_{xx}^2 - \sigma_{yy}^2}\right)\right]_2 - \left[\frac{1}{2}\tan^{-1}\left(\frac{2\sigma_{xy}}{\sigma_{xx}^2 - \sigma_{yy}^2}\right)\right]_1 \tag{4.17}$$

In the example we have used thus far, the evaluation of Equation (4.17) with the covariance values in Equation (4.5) yields a principle axis angle of 45-degrees for both ellipses, thus a difference of zero, meaning the ellipses are oriented along the same principle axis.

To show the effect on the norm of the updated covariance matrix, consider the following three covariance matrices, with the latter two being the same size but oriented along opposite axes:

$$\begin{aligned}\Sigma_1 &= \begin{bmatrix} 20 & 0 \\ 0 & 1 \end{bmatrix} \\ \Sigma_2 &= \begin{bmatrix} 1 & 0 \\ 0 & 10 \end{bmatrix} \\ \Sigma_3 &= \begin{bmatrix} 10 & 0 \\ 0 & 1 \end{bmatrix}\end{aligned} \tag{4.18}$$

Using Equations (4.4) and (4.13) we can test the combination of covariance ellipses 1–2 and 1–3 to show the full effect of aspect on the updated and how particular geometries reduce the position uncertainty better than others. The results are shown in Figure 13.

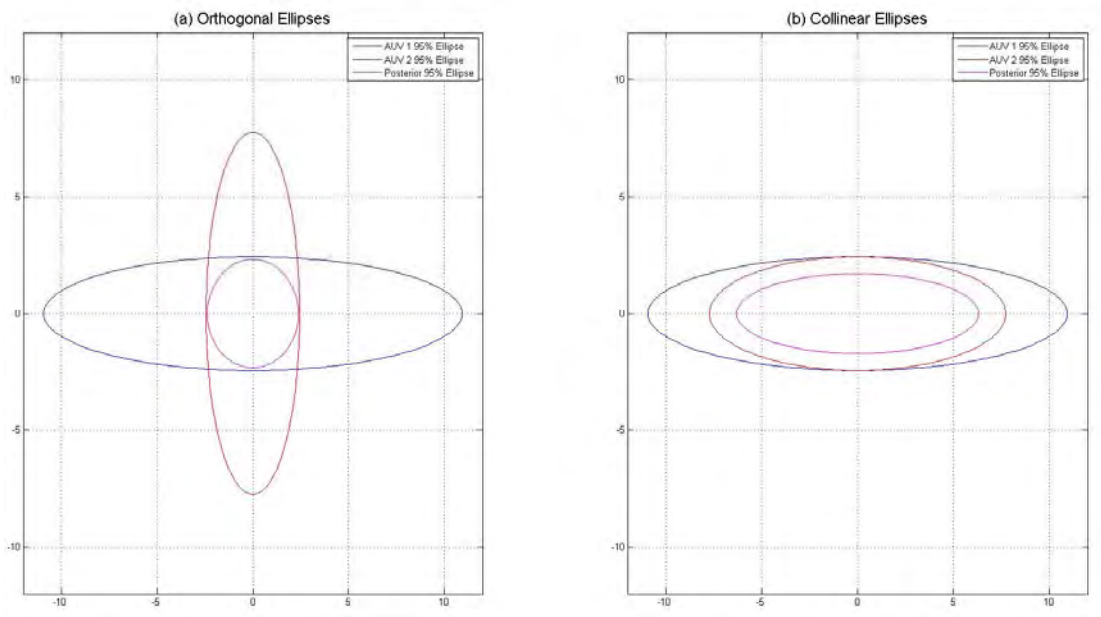

Figure 13. (a) The inferential results of two orthogonal, 95% ellipses as compared to (b) two collinear, 95% ellipses. The updated covariance matrix in (a) showed significant reduction (~93% by matrix norm) whereas the reduction in (b) is much more modest (66% by matrix norm) and still exhibits greater directional uncertainty in the x-direction.

Looking at the matrix norm indicates just how significant the reduction in position uncertainty is for the orthogonal case:

$$\begin{aligned} \left\| \Sigma_{k}^{1} \right\| &= 20.025 \\ \left\| \Sigma_{k+1|k}^{1,2} \right\| &= 1.3166 \\ \left\| \Sigma_{k+1|k}^{1,3} \right\| &= 6.6854 \end{aligned} \tag{4.19}$$

The orthogonal geometry produced a 93.4% reduction in matrix norm, compared to a 66.6% reduction in the collinear case. This simple example highlights the impact of geometry on position uncertainty reduction, which we can exploit to further our tactical security aims by only requiring aiding AUVs to transmit when the perceived reduction in position uncertainty for the other AUV exceeds a particular threshold.

D. ALGORITHM DEVELOPMENT AND INTEGRATION

Consider the postulated operational scenario of multiple AUVs mapping a minefield. At present, each AUV would be operating independently of the others to accomplish their assigned portion of the overall mission. There is no centralized control of the AUVs and each AUV is responsible for minimizing its own position uncertainty, thus maximizing local map accuracy. In the framework proposed below, the AUVs would have the ability to communicate acoustically to share position uncertainty information, enabling all AUVs to collaboratively keep position uncertainty low for the overall map of the area. The basic premise considers maximizing the information gain in that if an AUV exceeds a specified threshold, it will broadcast a message requesting assistance. The other AUVs will determine if their uncertainty information can assist the broadcasting AUV and transmit a reply if a threshold is met. This algorithm is fully distributed and decentralized. This section will describe the algorithm and its construction from a broad, operational-level view, and the key design features that optimize the relationship between position uncertainty and tactical security.

1. System Representation and Objectives

We begin with a schematic representation, Figure 14, which shows how we will use acoustic transmissions to reduce position uncertainty.

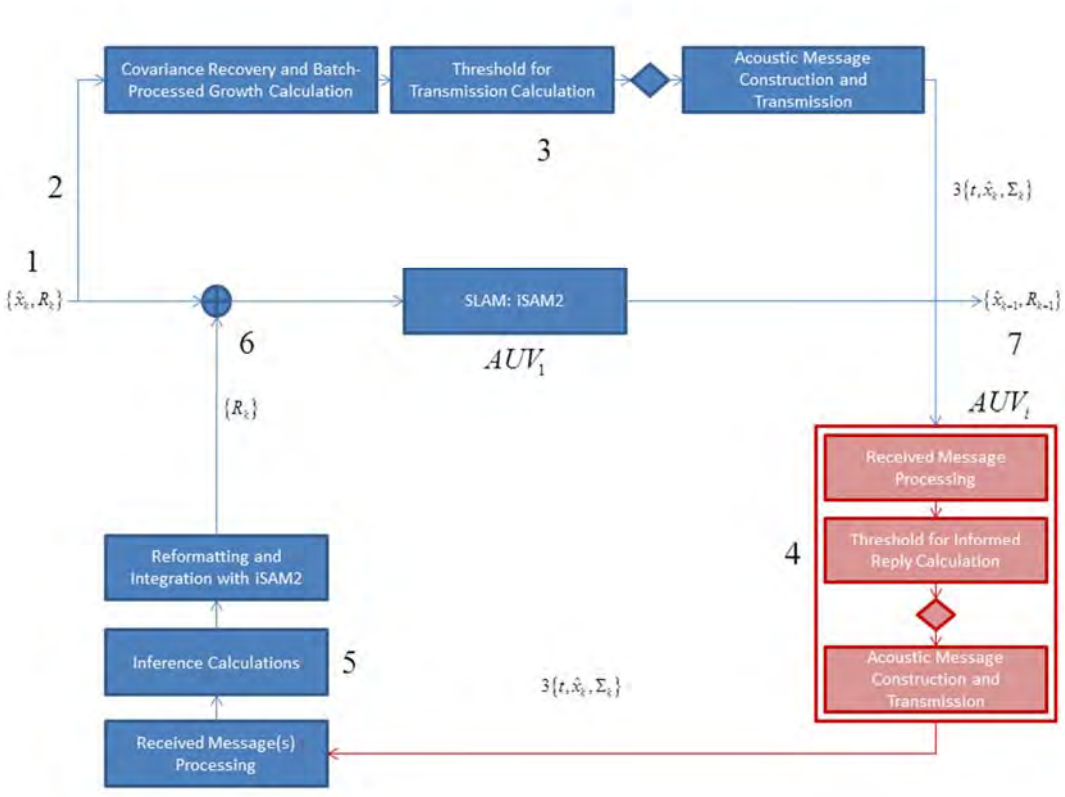

Figure 14. A schematic representation of the proposed algorithm to reduce position uncertainty through acoustic communications with an emphasis on tactical security concerns in Steps 3 and 4.

This recursive algorithm will operate in the following steps, external to the mechanics of iSAM2. This allows this algorithm to operate on a much broader set of SLAM algorithms.

1. The algorithm begins with the AUV pose and information matrix $\{\hat{x}_k, R_k\}$ at time k.

2. The information matrix R_k is sent to this algorithm for evaluation.

3. R_k is converted back into a standard covariance matrix. We extract the position variances and calculate the Frobenius norm. The norm is then compared to a moving average to determine the rate of position uncertainty growth over time. If it exceeds a specified threshold, the AUV

broadcasts a message requesting assistance from any autonomous vehicles in the area including its position and uncertainty information.

4. An AUV receives the broadcasted message, processes it, and determines if the inferential results of the two covariance matrices with the additional acoustic communications measurement covariance information will exceed a specified threshold for relative gain. If it does, it transmits a reply with its position and uncertainty information.

5. The broadcasting AUV receives the replies and processes them sequentially. Time domain multiple access (TDMA) considerations for deconflicting acoustic message transmission are assumed to be in place.[4] The received information is processed into the correct format to infer a updated covariance, which is then transformed back into an information matrix.

6. The updated information matrix is then reinserted into iSAM2 to be incorporated when the next pose node is created.

7. The process repeats.

The following subsections will elaborate on several of the design features of this algorithm and explain how the inferred information matrix will be integrated with iSAM2.

2. Measuring Covariance Growth and the Broadcasting Threshold

After the creation of a new pose node in iSAM2, we recover the covariance matrix using Equation (3.7) and extract the 2x2 matrix corresponding to the most recent pose node created, which correspond to position uncertainty, to form a new $2x2$ covariance matrix. We calculate the matrix norm with Equation (4.13) and store the values in an array.

[4] At this stage we may ignore the TDMA concerns based on the construction of the simulation model, but the issue of communications scheduling must be examined in future work to ensure that the assumption holds. Changes to the TDMA structure would not fundamentally alter the algorithm being developed here.

Once the length of the array includes thirty entries, we begin a moving average calculation between two windows of fifteen entries each, using the most recent thirty entries. The value was heuristically derived. The variable t indicates the current time step.

$$\begin{aligned} window_1 &= mean\left(\left\|\Sigma_1\right\|\left(1, t-30:t-16\right)\right) \\ window_2 &= mean\left(\left\|\Sigma_1\right\|\left(1, t-15:t\right)\right) \end{aligned} \tag{4.20}$$

Selecting an array length of thirty allows the initialization routines of the AUVs to settle out and the vehicle to travel a modest distance before enabling the remainder of the algorithm. Additionally, it provides a modicum of smoothing to prevent a single erroneous sensor measurement from triggering an acoustic transmission. Both aspects enhance tactical security be preventing excessive transmissions.

We then calculate the percent change between the moving averages:

$$\Delta\left\|\Sigma\right\|_{t|(t\ t-30)} = \frac{window_1 - window_2}{window_1} \tag{4.21}$$

If the percent change exceeds a specified threshold, the AUV will broadcast a message requesting assistance from other autonomous vehicles in the area. We will test for this threshold in simulation in Section V.

3. Threshold for an Informed Reply

Using the approach developed in Section IV.C.2, all receiving AUVs calculate the updated covariance matrix using information received in the broadcasted acoustic message, acoustic ranging data, and current uncertainty on the host vehicle. The AUV then calculates Equation (4.16) to determine the relative gain that the broadcasting AUV would realize if the host AUV's information were transmitted in reply. If the relative gain exceeds a given threshold, the AUV will transmit an acoustic message in reply. This approach reduces the number of vehicles transmitting while providing assistance to the broadcasting AUV and aids in deliberate or adaptive path planning to exploit the aspect dependence properties of the Bayesian inference.

4. Acoustic Message Construction and Packet Loss

The primer on ocean acoustics in Chapter II revealed the difficulties that we encounter in trying to communicate underwater. Paull, Seto, and Leonard [45] report that packet loss of 20–50% is not uncommon in this domain. Given our goal for minimizing the number of transmissions, the acoustic messages must be constructed to be more robust to packet loss, thus preventing additional transmissions. This aspect of the work will not be explicitly tested in the simulation framework presented in Section V, but contributes to the discussion on the use of acoustic communications for multi-AUV operations.

To account for this, each acoustic message will contain three copies of the information, including the timestamp, shown in Equation (4.22). Given the stochastic nature of acoustic communications, we heuristically deem it unlikely that two of the three values in any set of information will be corrupted, thus rendering the message unusable, otherwise the message would need to contain more than three repetitions of the same piece of information. While we prefer the message size to be less than 32 bytes for efficiency, we leave the analysis of this messaging technique to packet construction for future work.

$$\begin{aligned} msg_{desired} &= \left[t_{TOT}, \hat{x}_k, \Sigma_k \right] \\ msg_{actual} &= \left[t_{TOT}, t_{TOT}, t_{TOT}, \hat{x}_k, \hat{x}_k, \hat{x}_k, \Sigma_k, \Sigma_k, \Sigma_k \right] \end{aligned} \tag{4.22}$$

The receiving AUV can then process the received message and format it for further use in this algorithm as follows:

$$msg = \begin{bmatrix} t_{TOA} \\ Mode(t_{TOT}, t_{TOT}, t_{TOT}) \\ Mode(\hat{x}_k, \hat{x}_k, \hat{x}_k) \\ Mode(\Sigma_k, \Sigma_k, \Sigma_k) \end{bmatrix} \tag{4.23}$$

The WHOI micromodem will append the time of arrival (TOA) to the message, along with received signal characteristics (omitted from Equation (4.23) since it is not

relevant to this thesis). The AUV will then take the mode of each of the three information elements to build the message needed for follow-on processing.

5. Covariance Reduction

The estimation of the updated covariance proceeds according to the TDMA schedule in use. We apply Equation (4.11) to each message, forwarding the updated covariance after the first message into the next set of calculations. After each application of Equation (4.11), the algorithm will store the broadcasting AUV's pose and updated covariance information for reintegration with iSAM2. The use of iSAM2, a smoothing filter that considers all previous data during each iteration, allows for the insertion of these temporary features into the A matrix at the correct point in times, alleviating the framework from time latency issues.

6. Reintegration with iSAM2

For each AUV that replies, we can treat that transmission and its associated uncertainty as a feature node. In order to keep the map accurate, the communications nodes will be maintained in a separate database from the feature nodes. This allows the normal NLLS process to continue without requiring a new formulation of the system of equations.

However, at the time of publication, we have been unable to overcome technical difficulties encountered in the iSAM2 algorithm in MATLAB despite a concerted effort to do so and extensive dialogue with Dr. Michael Kaess. These issues stemmed from the conversion of the iSAM2 code from its native C++ environment into MATLAB that had heretofore gone undiscovered. As a result, we will still utilize the iSAM2 framework for SLAM operability, such as navigation and mapping. Reintegration of covariance reduction will be demonstrated through the use of a generic covariance function that mirrors SLAM performance.

Section IV described the algorithmic framework for using acoustic communications to reduce position uncertainty of a requesting AUV. It considered the

operational level implementation and discussed the various aspects of the algorithm from a systematic approach. It introduced the concept of a Bayesian inference as a way of fusing two measurements into an updated estimate of covariance and discussed measuring the relative value or performance of two covariance matrices using an application of Kullback-Leibler divergence from information theory.

V. SIMULATION AND ANALYSIS

A. OVERVIEW

This thesis considers the value of acoustic communications in MVSLAM operations in reducing position uncertainty of a particular vehicle. To test the theoretical framework proposed in the previous section, we will conduct simulations to collect the data necessary to answer the following research questions.

- How can we minimize acoustic communications while achieving acceptable performance in terms of position uncertainty? What constitutes acceptable performance in light of tactical security considerations?
- What should the threshold be for transmitting an acoustic message, both in broadcast for assistance and in replying to broadcasts?
- Can we minimize the need for GPS fixes?
- What is the value of acoustic communications for underwater MVSLAM?

B. EXPERIMENTAL CONSTRUCTION

1. Operational Area

To make this work readily adaptable for in-water testing, we have selected a simulation area that corresponds geographically to the marina in Monterey Bay, shown in Figure 15.

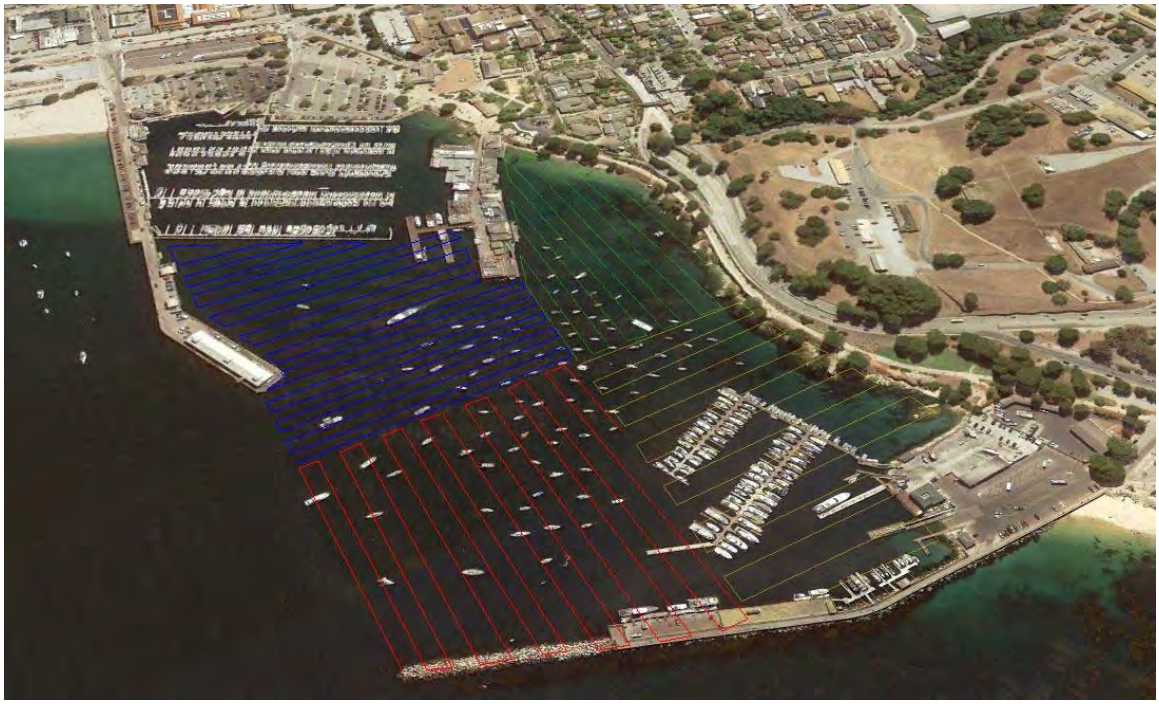

Figure 15. A satellite image of the public marina in Monterey Bay, California, with hypothetical vehicle tracks overlaid.

We utilize a traditional search pattern, colloquially known as a "lawnmower" pattern to ensure that we fully search and map an area. We utilize four AUVs, but the approach described in this thesis should scale to *n*-number of AUVs.[5] The simulation area shown in Figure 15 has been translated into a simulated MATLAB environment, shown in Figure 16. It consists of a four square kilometer area partitioned into one square kilometer search areas. Track spacing for the AUVs is set at 20 meters to ensure 100 percent FLS coverage in the search area, with approximately 15 percent overlap.

[5] In theory the application of the Bayesian inference will scale to *n*-number of AUVs, but this will operationally be limited by the TDMA schedule in place. TDMA concerns are not relevant to this thesis but will factor into the operational implementation of this framework for large numbers of AUVs.

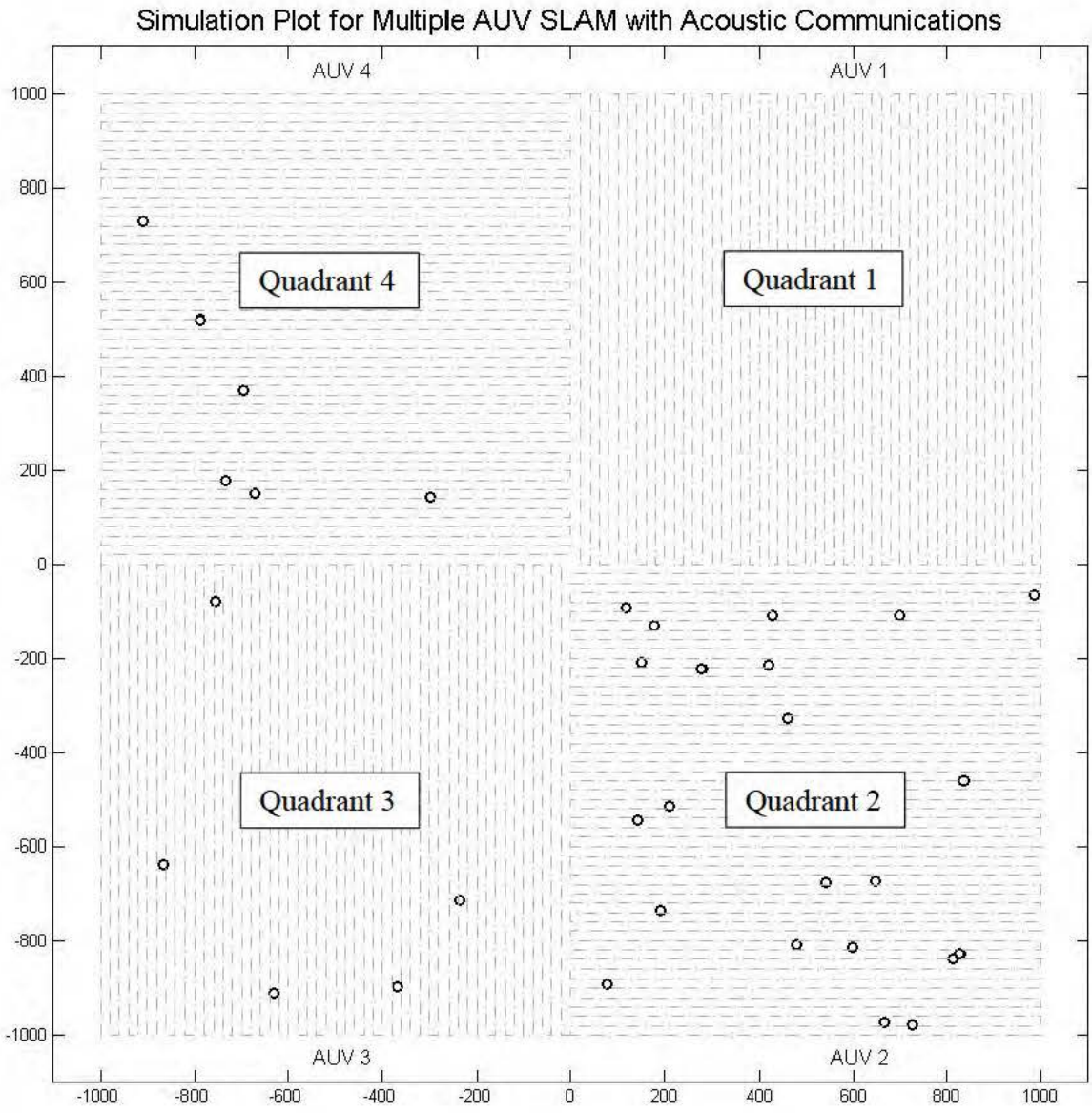

Figure 16. A map of the simulated search environment with the navigation tracks for 4 AUVs overlaid. The red tracks indicate a search in progress. Each of the four labeled quadrants has a different feature density. The feature density will be varied across simulations.

2. Simulation Variables

The simulation employed in this thesis maps the notional operational area. All AUVs are considered to be identical to the REMUS 100 AUVs outline in Section II.A. Future work can and should consider the variation of vehicle-specific parameters, such as

INS or FLS accuracy, on this framework. However, for this thesis, we only consider a few independent variables, presented in Table 3 with brief explanations. These parameters will remain at the given values unless stated otherwise.

Table 3. The independent simulation control variables as related to determining the performance of acoustic communications in MVSLAM operations.

Variable	Initialized Value
Time Delay The time elapsed before the acoustic communications framework becomes active for the AUVs.	200 seconds
Reset Time The time required to elapse between acoustic broadcasts to allow for system stabilization.	50 seconds
Reply Threshold The required reduction in position uncertainty required to transmit a reply to an acoustic broadcast.[6]	20-90 percent
Minimum rms Average[7] The minimum, average rms value required to enable acoustic broadcasts.	0.5 meters
Moving Window Size The number of rms average values to be included for percent growth calculations to trigger an acoustic transmission.	90 seconds

[6] The reduction is based on the application of Kullback-Leibler divergence discussed in Section IV.C.2.b.

[7] The rms average of the time-indexed covariance matrix norms. This parameter will be more fully discussed in the next section.

3. Measures of Effectiveness and Performance

Interpreting the change or rate of change in a covariance matrix requires the considered reduction of a four-element matrix into a single value. Equation (4.13) provides the reduction using the Frobenius norm. However, to monitor performance over time and reduce the impact of oscillations in algorithm performance, we must also consider a more time-weighted metric. To achieve this, we calculate the rms average of the stored, time-indexed Frobenius norm values. This approach yields two principal benefits. First, it dampens localized oscillations within the algorithm and thus provides a better indication of system performance over time. Second, it provides a mechanism by which we can define the system performance trade space and make direct comparisons to INS-only solutions, with GPS fixes at various finite intervals. The rms average should be thought of as a single number characterizing the average position uncertainty at time *k*. Going forward, the rms average of the time-indexed covariance matrix norms will be truncated in writing as the rms average.

4. Simulation Plan

This simulation plan creates the framework to collect the empirical data needed for answering the research questions posed in Section I and again at the start of this section. The answers to the research questions need to be derived from two distinct bodies of data, and thus the simulation plan is partitioned into two phases in order to test the appropriate variables and extract the necessary data.

First, we must understand the performance of current systems, including both SLAM and INS-only algorithms. Defining this trade space allows us to determine what constitutes acceptable performance in this field. At a minimum, the results of this thesis must be no worse than the existing operational constructs. To establish this performance baseline, we will serially vary two parameters: GPS fix interval and feature density. The GPS fix interval will establish the INS-only system performance. We examine six different GPS fix intervals: 15, 30, 45, 60, 90, and 120 minutes. Varying the feature density from featureless to well-featured will establish the range of the performance metrics for the existing iSAM2 SLAM architecture. The feature density will range from

0–42 features per square kilometer in 6-feature increments. The GPS data, since it does not depend on a random process, will be collected through two simulation runs with each quadrant utilizing a different fix interval. For the feature density analysis, we will conduct multiple simulations, varying the feature map with randomly-distributed features each time. Each feature density will have twelve simulation runs.[8] The collection of data on these two parameters will define the upper and lower bounds on system performance needed to evaluate the contribution of this thesis.

Second, with the results of the first phase of simulation testing in mind, we must systematically test the communications architecture to produce the maximum acceptable performance whilst maximizing tactical security by minimizing the frequency of acoustic communications. To accomplish this, we will vary the variables presented in Table 3 specifically the reply threshold to produce heuristically-optimal performance. The broadcast threshold will be set on logic-based condition of two parameters: the rms average performance of the vehicle compared to the INS-only solution and the rms average performance being above the minimum rms average value.

At this stage of the research, the qualitative nature of tactical security precludes the use of numerical optimization techniques and thus an analytically-derived answer for broadcast-reply settings will be used. The performance of the AUVs between the two sets of simulations will inform the tactical security analysis. These simulations will be conducted in environments with randomly-distributed features to significantly reduce unintentional correlations of system performance with a particular feature layout.

C. SIMULATION CONSTRUCTION

1. Performance Baseline Determination

We begin the experimental plan by determining the trade space that AUVs conducting SLAM operations function in. By bounding this trade space, we allow for a more accurate assessment of acceptable performance for broadcast-reply thresholds. Table 4 shows the feature density and GPS fix interval assigned to each quadrant for each

[8] A true Monte Carlo simulation would be best, but time constraints did not permit a sizable number of trials to be conducted.

of the two simulation sets. Each set will be run 12 times to ensure sufficient randomization of features.

Table 4. The assignment of feature densities and GPS fix intervals for the first two sets of simulation runs. The runs will collect the performance metrics necessary to define the trade space for SLAM operations.

Quadrant	Feature Density [#/km^2]	GPS Fix Interval [min]
Set 1		
1	0	15
2	6	30
3	12	45
4	18	60
Set 2		
1	24	90
2	30	120
3	36	Not Required
4	42	Not Required

To give a perspective on how the feature density manifests in the simulation area, Figure 17 and Figure 18 are provided to show the feature densities for the first and second simulation runs given in Table 4.

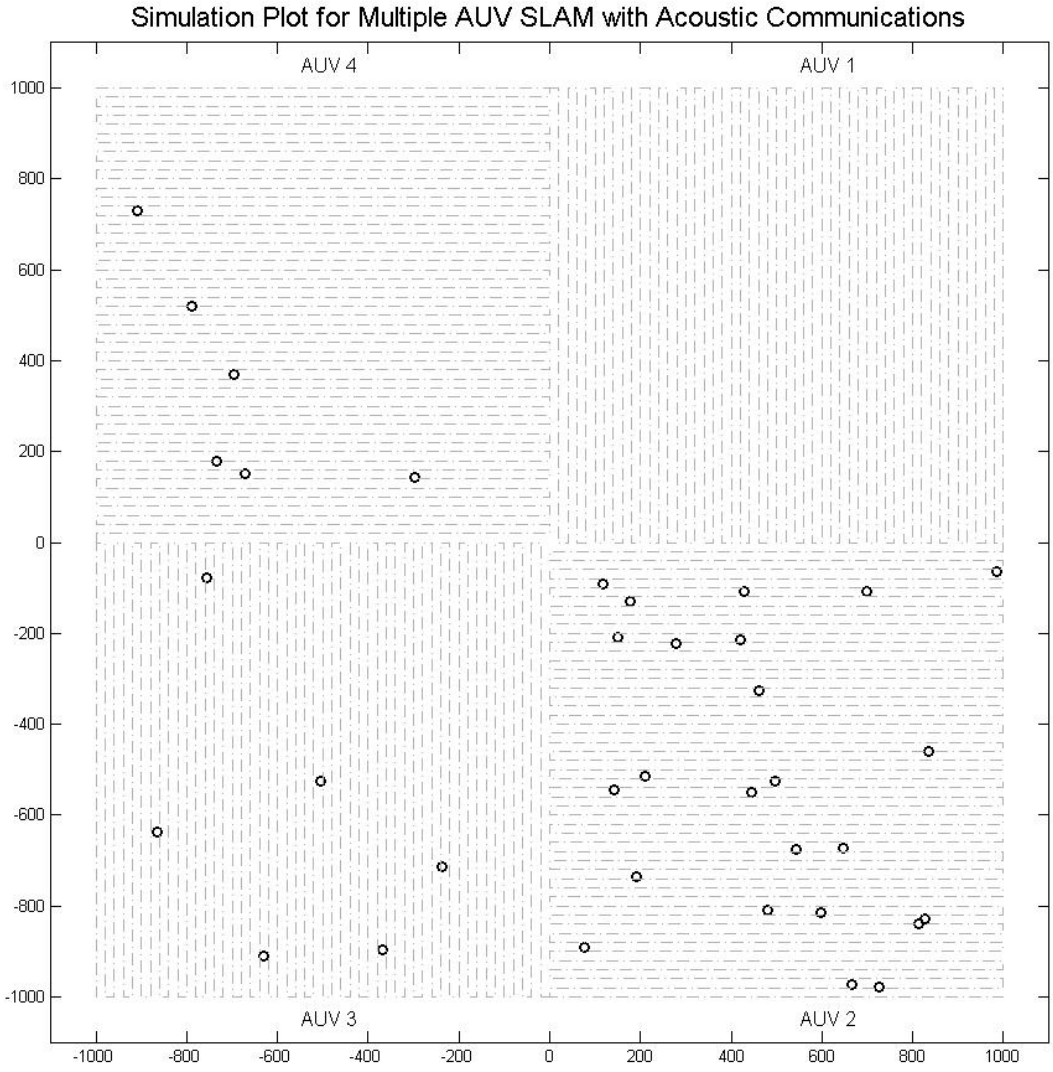

Figure 17. The simulation plot with varying feature densities by quadrant. Quadrant 1 is featureless, Quadrant 2 has 6 features, Quadrant 3 has 12 features, and Quadrant 4 has 18 features.

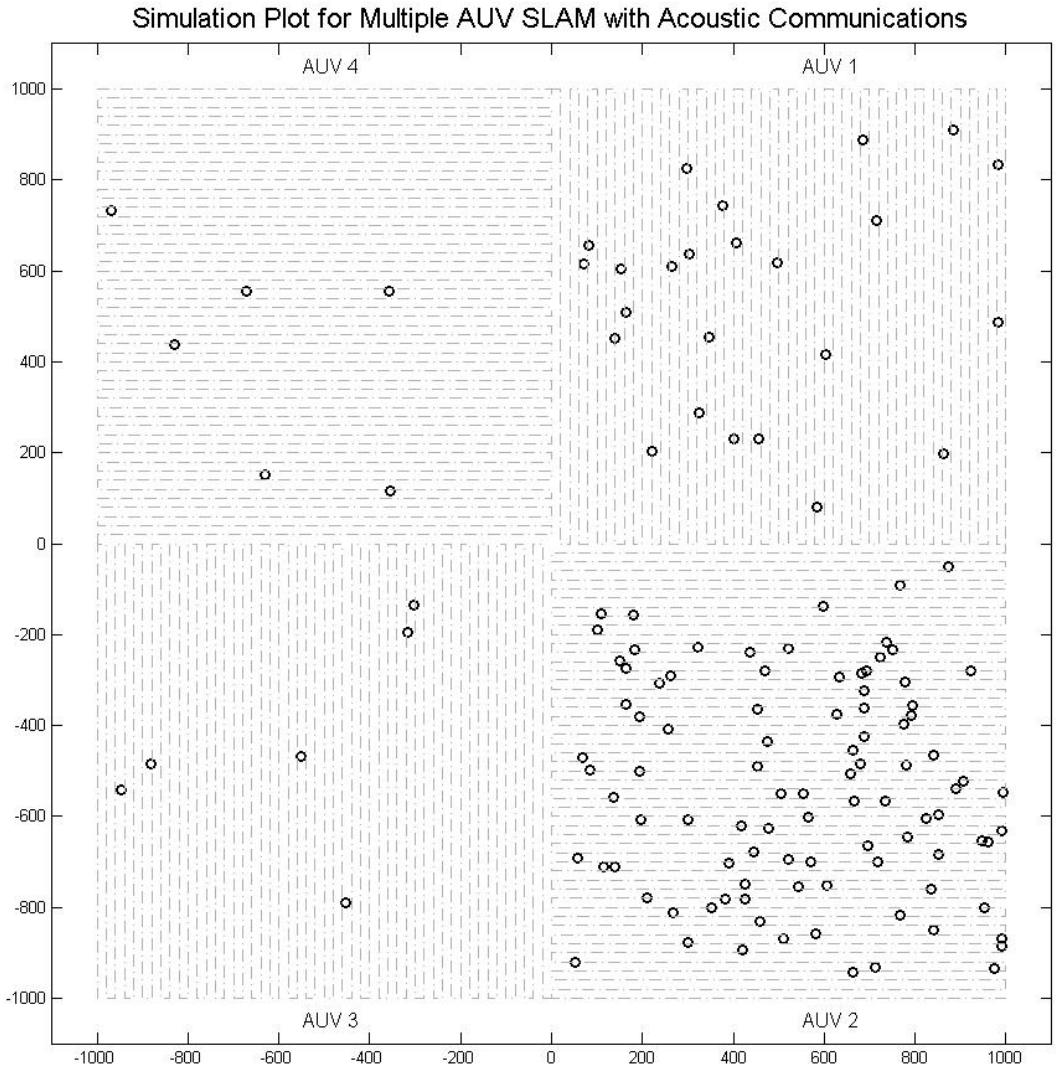

Figure 18. The simulation plot with varying feature densities by quadrant. Quadrant 1 has 24 features, Quadrant 2 has 30 features, Quadrant 3 has 36 features, and Quadrant 4 has 42 features.

2. Threshold Determination

The second aspect of the simulation plan explores the threshold for replying to a broadcast for help. Our emphasis on tactical security requires this analysis. To accomplish this, we will fix the feature density and GPS intervals as shown in Table 4 and Figure 19.

Table 5. The fixed simulation parameters of feature density, by quadrant, and GPS fix interval for the threshold determination runs.

Quadrant	Feature Density [#/km^2]
1	0
2	12
3	30
4	42
GPS Fix Interval: 60 min	

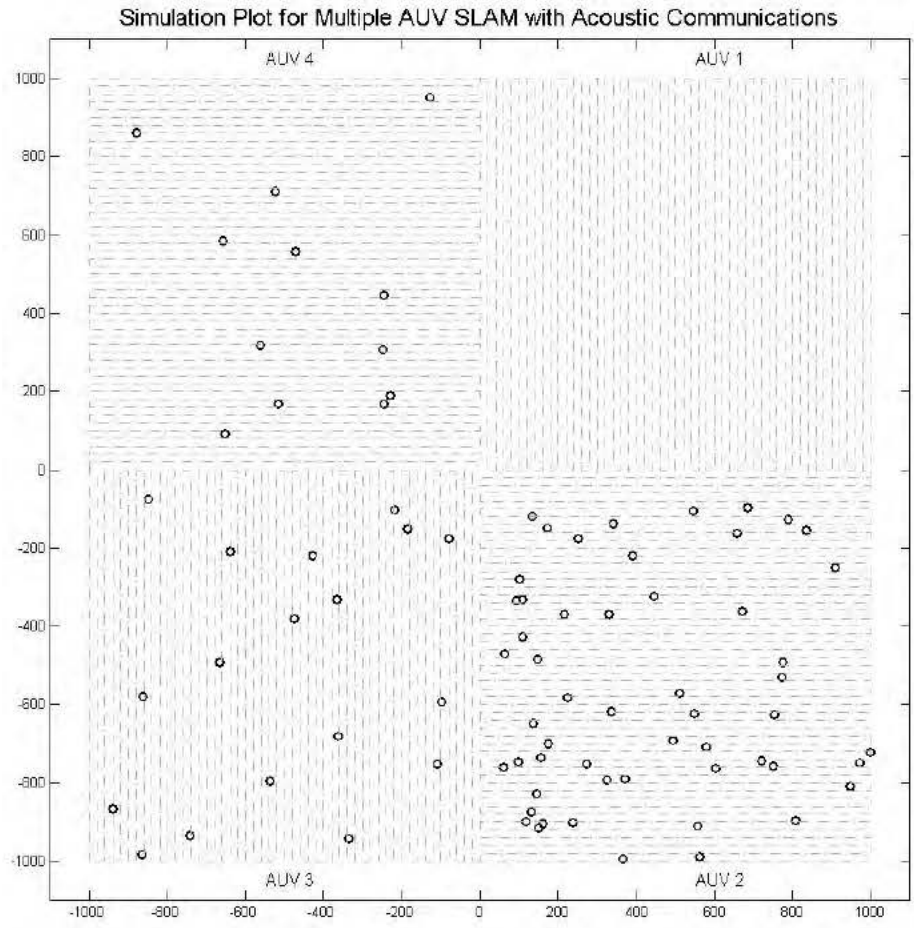

Figure 19. The simulation plot for the threshold evaluation with the given feature densities. Quadrant 1 is featureless, Quadrant 2 has 12 features, Quadrant 3 has 30 features, and Quadrant 4 has 42 features.

This feature density arrangement was chosen to force one AUV, in quadrant 1, to communicate periodically. The absence of features will drive an INS-only SLAM solution. The remaining feature densities were selected to explore the relationship between feature density and the ability to effectively reduce another AUV's position uncertainty. We will conduct three simulations for each of the threshold values.

The broadcasting AUV will transmit when the average rms value is greater than 0.50 meters and the rms average approaches or exceeds the INS-only value. As explained in Section IV.D.3, any AUVs receiving a broadcast for assistance will process the message and calculate the percentage reduction that would occur if the receiving AUV transmitted a reply. Therefore, we set this part of the experimental plan to evaluate the various transmission thresholds for an informed reply. We will evaluate in increments of 10 percent from 20–90 percent possible reduction.

D. RESULTS AND PERFORMANCE ANALYSIS

1. Performance Baseline Determination

We evaluated the GPS fix interval and feature densities using the simulation model described previously. This section will discuss the applicable performance parameters of both the GPS fix interval and feature density analyses and their implications for threshold determination.

For GPS fix interval, the performance overtime will resemble a sawtooth pattern as the uncertainty grows over time and is eventually reduced with a GPS fix. The rms average of this sawtooth pattern, a partial consideration for the threshold determination in the next section, as a mathematically closed-form answer:

$$avg_{rms} = \frac{Amplitude}{\sqrt{3}} \tag{5.1}$$

We tested this analytical solution in simulation using fix intervals of 15, 30, 45, 60, 90, and 120 minutes, shown in Figure 20.

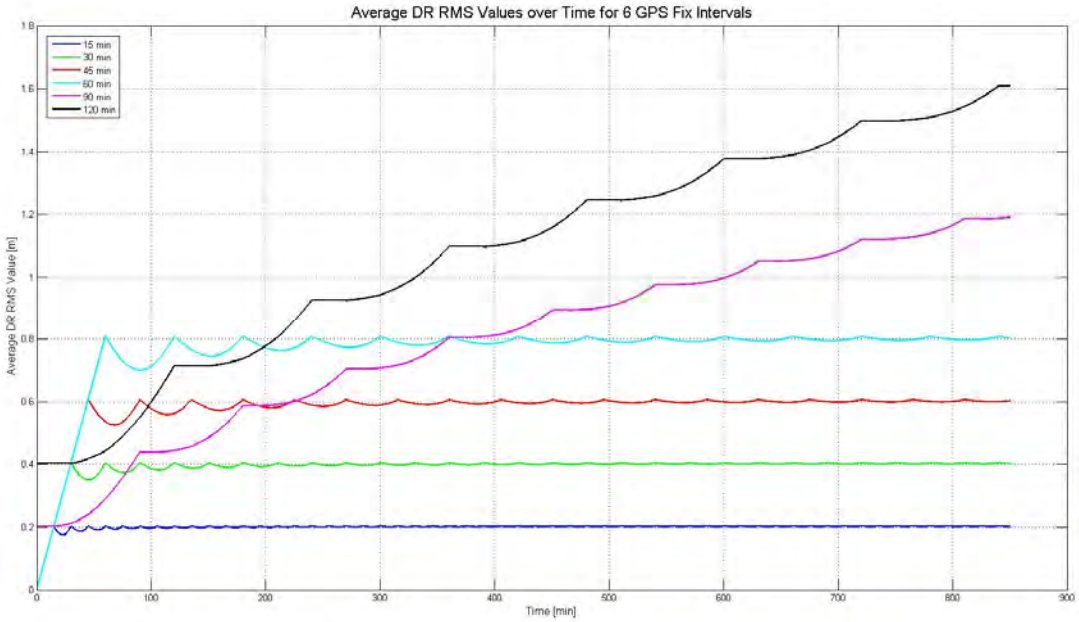

Figure 20. The rms average of the time-indexed covariance matrix norms for six GPS fix intervals: 15, 30, 45, 60, 90, and 120 minutes. The values converge or begin to show convergence to the predicted analytical solutions for the rms average of a sawtooth wave.

Figure 20 shows the rms averages converging to the analytical solution in Equation (5.1) as expected. This data aids in defining the trade space that we will work from to heuristically determine the threshold values. The GPS fix interval for the NPS REMUS vehicles can be manually set to any interval. We default to 30 minutes in practice.

Second, we evaluated SLAM algorithm performance across eight feature densities to assess performance in terms of both covariance, which correlates directly with map accuracy, and the rms average of the covariance matrix norm, which provides a more stable indicator over time. Figure 21 and Figure 22 show the averaged results of the 12 simulation runs in terms of covariance and the rms average of covariance, respectively.

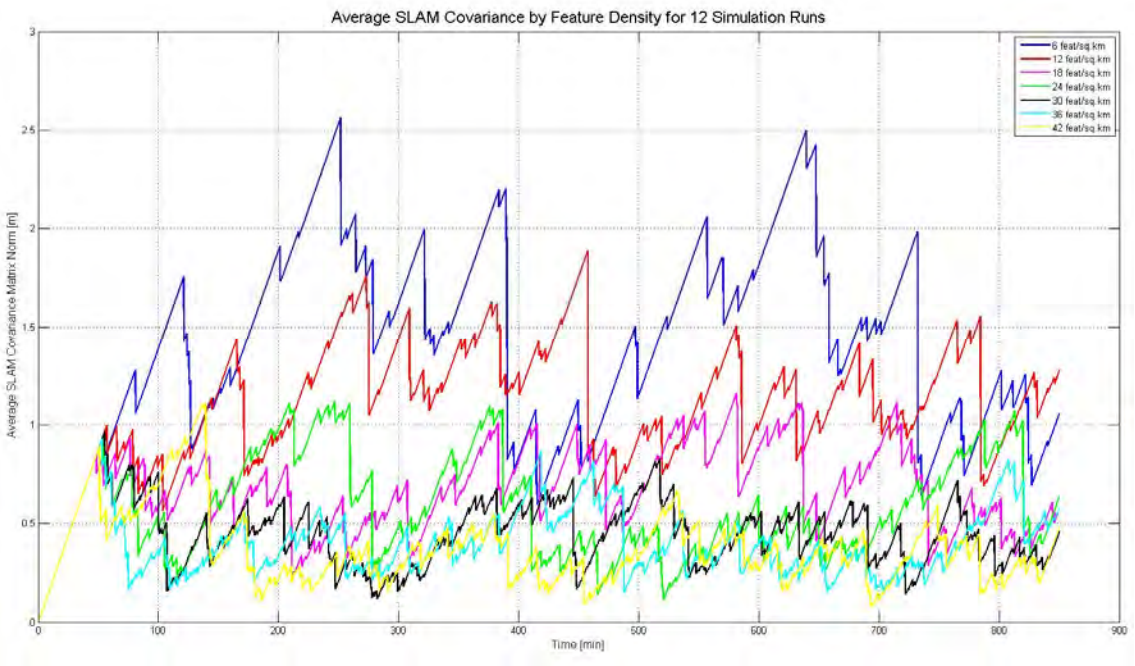

Figure 21. Average covariance matrix norms from 12 simulation runs in each of eight different feature densities.

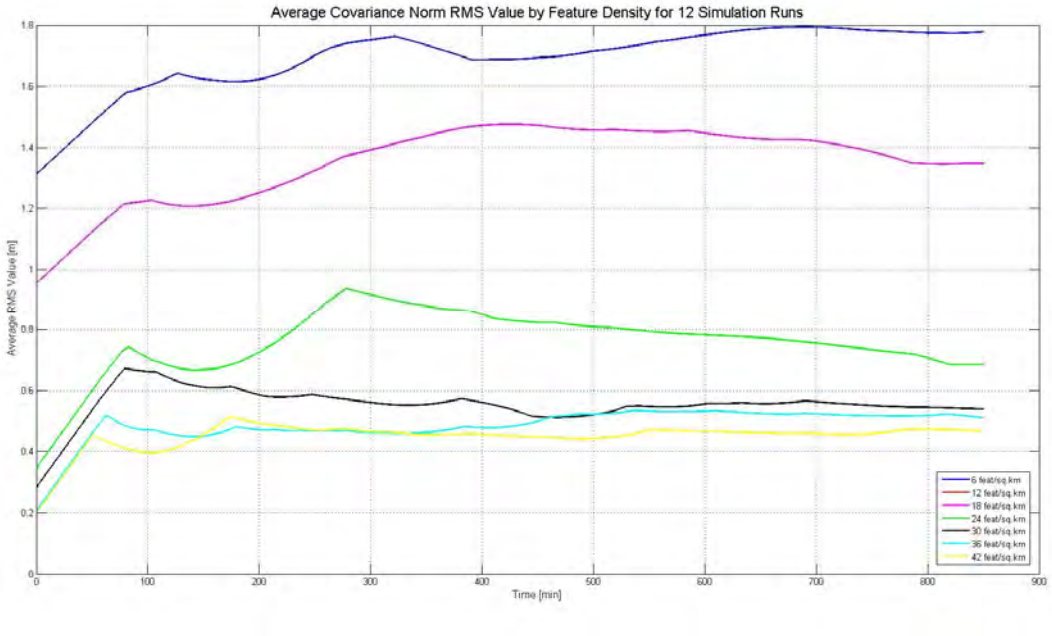

Figure 22. The rms average value of the covariance matrix norms from 12 simulations runs in each of eight different feature densities.

Figure 22 provides significant insight into SLAM performance across different feature densities. We can see that the performance does not improve appreciably once the number of features exceeds 30 features per square kilometer. In the future this will allow for adaptive search planning by multiple AUVs to ensure that search areas can be adaptively reassigned to allow balancing of features between AUVs. This will stabilize the overall position uncertainty for the AUV flight and improve map and navigational accuracy since each AUV will individually have better SLAM solutions following area reassignment.

To determine what constitutes acceptable performance, we combined the results from the GPS fix interval and feature density analyses into a common plot. Figure 23 shows the rms average of the covariance matrix norms over time for four feature densities and four GPS fix intervals.

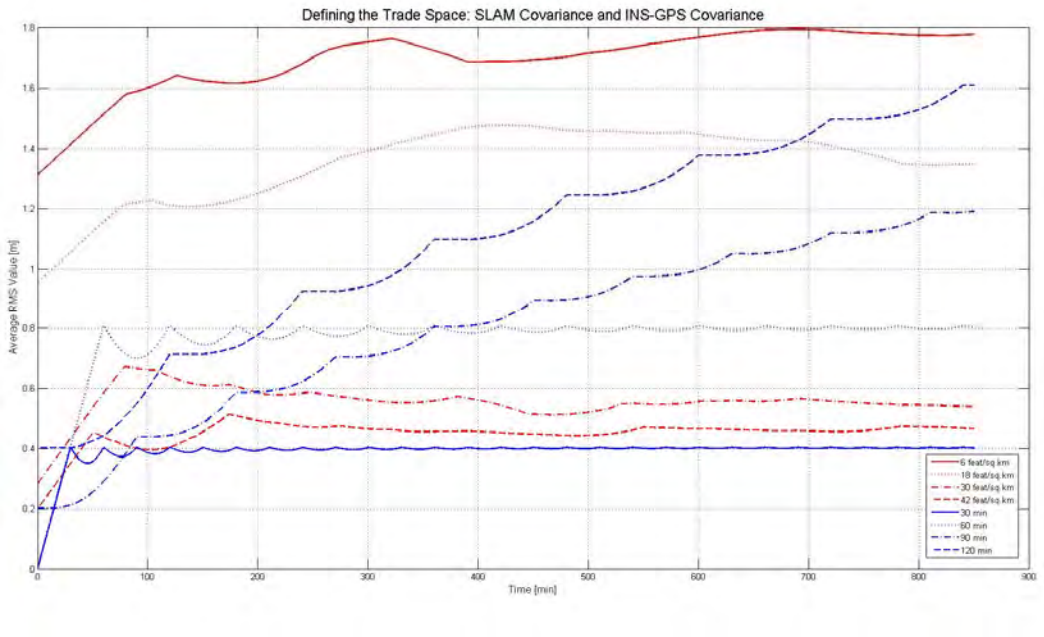

Figure 23. The rms average values of the covariance matrix norms for four feature densities and four GPS fix intervals. The feature densities are 6, 18, 30, and 42 square kilometers and the GPS fix intervals are 30, 60, 90, and 120 minutes. This figure defines the performance trade space for a reply threshold determination.

As stated previously, the goal is to provide acceptable, not optimal, performance. The 30-minute fix interval represents the lower bound in Figure 23. This fix interval is operationally burdensome in a well-featured area, akin to the SLAM results for 30 and 42 features per square kilometer, since the vehicle will have to cease mapping, surface, obtain a GPS fix, submerge, and regain track. In the context of a minefield neutralization problem, this means the vehicle also has to reacquire the field and localize itself to ensure the correct mine is targeted. Given that burden, we relax the GPS fix interval to 60 minutes to provide greater flexibility and accommodate a wider range of feature densities. The rms average for the 60-minute fix interval provides the upper bound on the acceptable performance envelope. Thus, SLAM performance with an rms average greater than 0.8 meters we reject as unacceptable.

The lower bound will govern the minimum uncertainty threshold for broadcasting. To prevent excessive acoustic communications, a tactical security concern, we set the minimum rms value for transmission at an rms average of 0.5 meters or greater. SLAM performance may achieve better results than this, meaning the AUV will not need to communicate because the SLAM performance alone meets or exceeds our acceptable performance standard.

We will implement the upper and lower bounds algorithmically by using logical comparisons. The broadcasting AUV will transmit an acoustic message requesting assistance from other AUVs in the area if the following two conditions are met: 1) the time-indexed rms average of the broadcasting AUV's covariance matrix norm is greater than the specified minimum rms value of 0.5 meters; and 2) if the time-indexed rms average is greater than the INS-equivalent rms average minus 0.25 meters.

An additional result to those presented in this section involves the standard practice of using finite GPS fix intervals. Figure 22 and Figure 23 show that, as long as the AUV is detecting features periodically, defining a modestly-featured environment, the performance in terms of position uncertainty will be acceptable. In this case, the GPS fix interval can and should be shifted from a finite interval to a variable interval based on the predicted position uncertainty. This will provide greater operational efficiency by

minimizing the time spent ascending and descending for GPS fixes and reduce the probability of counter-detection when the AUV is at the surface.

2. Broadcast-Reply Performance

The reply threshold is based on the possible percent reduction for the broadcasting AUV if the replying AUV were to transmit its position and covariance information. In an effort to minimize acoustic communications and still achieve acceptable performance, we varied the reply thresholds in ten percent increments from 20–90 percent and measured the performance parameters. We consider the performance of the broadcast-reply threshold in terms of the average number of acoustic transmissions by an AUV for the given threshold value and by the average percent reduction achieved for the given threshold value.

Intuitively, we would expect the number of transmissions to increase with a lower threshold for reply. However, as Figure 24 shows, the number of transmissions actually increases as the threshold for reply gets larger. This results from the fact that the replying AUVs may not be able to meet the higher threshold, leaving the broadcasting AUV transmitting acoustic messages more often requesting assistance.

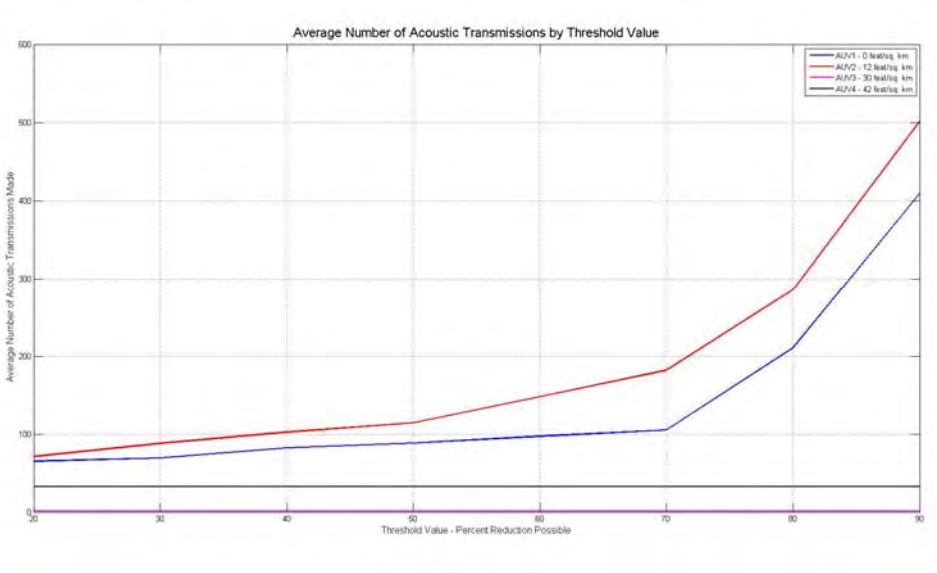

Figure 24. Average number of acoustic transmissions by possible percent reduction threshold value for each AUV. The average is across three simulations for each threshold value.

In terms of the percent reduction, we again analyze the average percent reduction by threshold value from the three simulations. The results are shown in Figure 25.

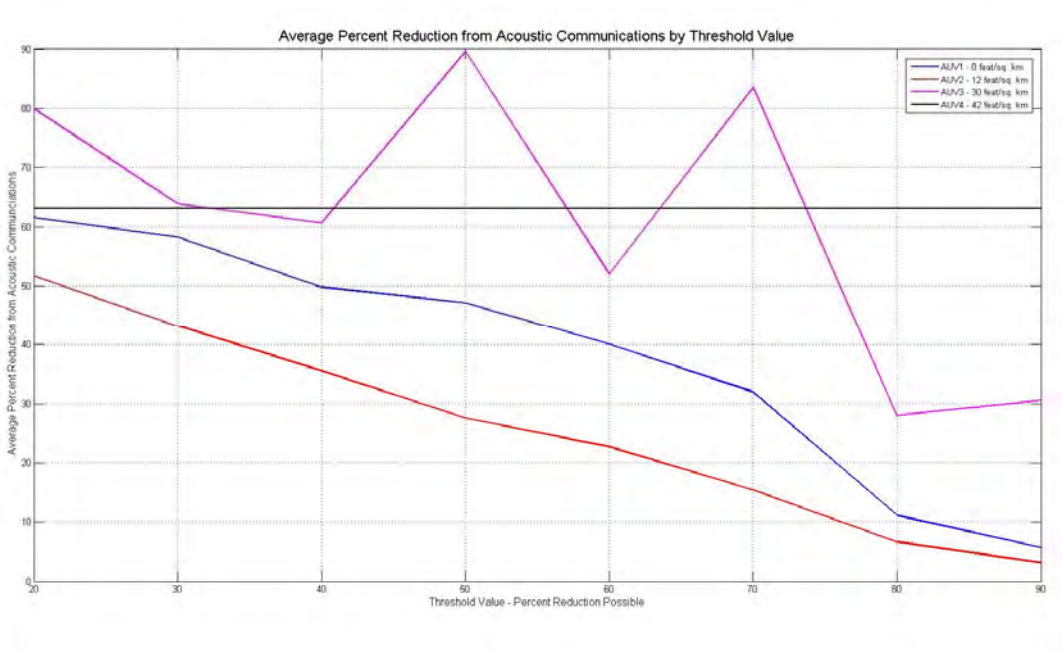

Figure 25. Average percent reduction from acoustic communications by possible percent reduction threshold value. The average is across three simulation runs at each threshold value. In poorly featured environments (red and blue lines), the trend is clear. In modest to well-featured environments (magenta line), the small number of simulations did not smooth the data sufficiently to draw conclusions. The black line represents the fourth AUV, which did not communicate.

We again see overall higher percent reduction at the lower threshold, especially for the AUVs operating in poorly featured environments, the red and blue lines in Figure 25. The small number of simulations did not provide sufficient smoothing of the data for the two AUVs operating in the well-featured environments, but their performance as previously been defined as acceptable and thus do not factor into this analysis.

The decreasing trend in Figure 25 can be attributed to the greater capacity for an individual AUV to reply to the broadcast for assistance. As we demonstrated in Section IV.C.2 on the utility of the Bayesian inference, the greater number of replies will result in a higher overall reduction. The higher threshold value thus bars other AUVs that could

provide meaningful reduction from assisting the broadcasting AUV, limiting the effectiveness of the acoustic communications framework presented here.

The performance of the AUVs at the 20 percent reply threshold is given in Figure 26.

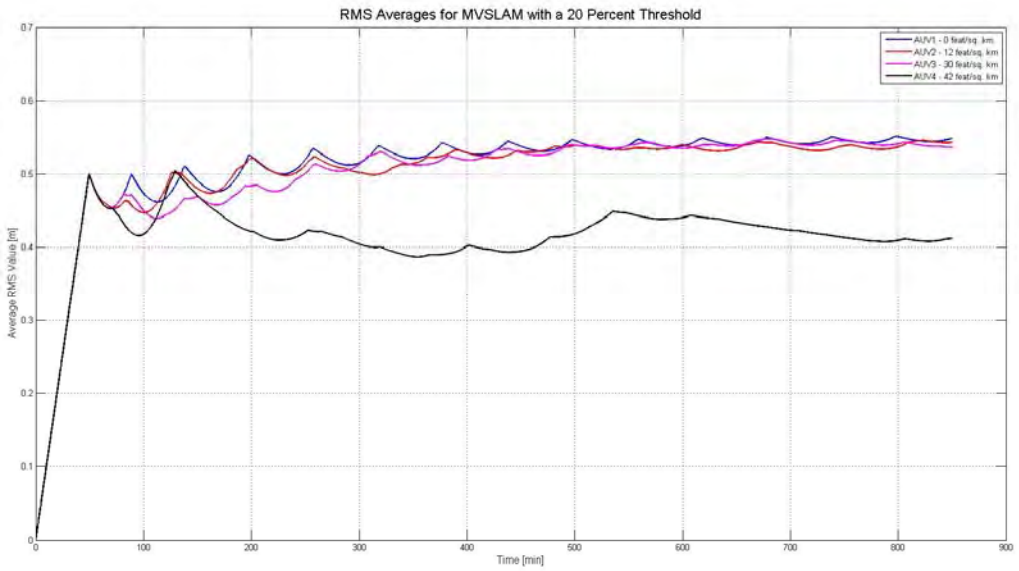

Figure 26. RMS average values of the time-indexed covariance matrix norms for four AUVs using a broadcast-reply acoustic communications scheme with a 20 percent possible reduction reply threshold.

In comparing Figure 26 to Figure 22 and Figure 23 we can see that this acoustic communications framework produced acceptable performance as we previously defined it. AUV 4 was in a well-featured area and did not require acoustic communications to reduce position uncertainty. However, the other three AUVs all benefitted from the acoustic communications framework and were able to improve their position uncertainty to values greater than the SLAM algorithm alone would have produced for each of the feature densities.

E. VALUE OF ACOUSTIC COMMUNICATIONS

The results of the simulations indicate unequivocally the efficacy of the acoustic communications framework proposed in this thesis. We recommend setting the reply

threshold at the lowest possible value to allow the greatest number of AUVs to render assistance while minimizing acoustic communications. This is in keeping with the principles of tactical security that require us to limit acoustic communications in order to prevent counter detection of the acoustic signals and maintain the operation covert.

Section V articulated the simulation model and plan and presented and discussed the results. We sought to answer the questions posed at the beginning of the section on how to minimize acoustic communications while achieving acceptable performance, minimizing the need for GPS fixes, and determining the informed threshold for reply in the broadcast-reply framework developed in Section IV. We found that acoustic communications do add significant value to multiple-AUV operations. Additionally, we explored the effect of feature density on SLAM operations and discovered the possibility of gaining greater operational efficiency by shifting from finite to variable GPS fix intervals.

THIS PAGE INTENTIONALLY LEFT BLANK

VI. CONCLUSIONS AND FUTURE RESEARCH

A. CONCLUSIONS

1. Major Results

The simulations and analysis of the proposed acoustic communications framework shows the validity of a multi-vehicle distributed system approach to reducing position uncertainty in underwater navigation. We traded optimal performance for acceptable performance and constructed the acoustic communications broadcast-reply framework based on that metric. Through simulation we determined that a low threshold of informed reply produces fewer acoustic transmissions while giving the greatest percent reduction of position uncertainty. We also gained greater insight into the effect of feature density on the performance of SLAM algorithms and found a potential ability to shift from finite to variable GPS fix intervals.

Additionally, the framework developed in this thesis can be extrapolated to a large number of AUVs, thus providing greater flexibility to operational commanders.[9] A system of AUVs has the ability to share position information and collaboratively reduce their own position uncertainty and increase map accuracy. This increases mission effectiveness by increasing coverage, reducing mission time, and improving system robustness through the use of multiple AUVs.

2. Contributions

SLAM frameworks have traditionally only utilized expropioceptive sensors for measurements. The use of the acoustic modem indicates that there may other non-traditional sensors that can help improve SLAM algorithm performance by adding temporary features. We evaluated the SLAM algorithms through the lens of tactical security. The tactical aspects of acoustic communications are an important parameter for multi-vehicle collaborative navigation and operations. This aspect of acoustic communications and SLAM has, to this author's knowledge, never been explored before.

[9] As previously mentioned, this conclusion is predicated on handling the TDMA scheduling concerns.

We developed an information-theoretic framework consistent with optimal estimation for minimizing system navigation and mapping errors that is not reliant on external beacon or positioning systems. Lastly, we developed a simulation model to address the various model parameters that affect the effective deployment of a multi-vehicle system engaged in underwater navigation and mapping operations. This included a brief analysis of aspect dependence as a means of achieving greater uncertainty reduction and is a key parameter for adaptive search and path planning in future work.

3. Limitations and Issues

The simple acoustic communications framework developed and presented here does have several limitations. First, the framework can only succeed when AUVs are within communications distance of each other. Second, the use of another AUV's covariance information to reduce position uncertainty does introduce cross-correlation into the global covariance matrix. The introduction of cross-correlation terms will jeopardize the independence assumption that underpins the probabilistic framework. That was not accounted for in this thesis and must be analyzed as a matter of future work. We did not construct the architecture to allow for other reply AUVs to reduce their position uncertainty from other received replies. The omnidirectional nature of acoustic communications means that each AUV that replies has the ability to receive the other replies and use those messages to reduce their own position uncertainty, even if it meets or exceeds the acceptable performance standard defined in this thesis.

B. FUTURE WORK

This thesis considered a very narrow segment in the nexus between acoustic communications and underwater MVSLAM operations. Given that narrow scope, we necessarily leave several next steps to future researchers.

- How is the independence of covariance matrices affected by acoustic communications between vehicles?
- How can we use this implementation to induce loop closure in SLAM?

- What are the proper contents for the acoustic message to keep the size under 30 bytes while still achieving the required single-transmission success metric?
- How can this implementation evolve adaptive path planning and mapping?
- How can we leverage any transmissions to create a communications map of the environment?
- How can we use acoustic communications to distribute highly accurate position information to a group of AUVs, such as when a single AUV obtains a GPS fix?

C. APPLICATIONS

The algorithm for acoustic communications in support of underwater MVSLAM operations applies specifically to the operational environments detailed in Section I, but we can also draw greater value by expanding the view of this thesis to a much broader level. This thesis implemented the novel consideration of an acoustic transmission as an independent measurement, not simply a communications path. The value taken from both the transmission itself and the information contained in the transmission enabled us to reduce the position uncertainty of an AUV, thus enabling greater operational flexibility and enhancing tactical security. Taking this idea more abstractly, we can see the inherent value of using non-traditional sensors to better localize a ship's position in an A2/AD environment. In the future, this may consist of a ship launching an AUV to obtain a precise position fix in a well-featured or contoured environment that the ship cannot enter into or a submarine utilizing other sensors, such as a fathometer, mapping sonar, or periscope, to obtain position information and thus reduce position uncertainty. The ability of our forces to sufficiently localize their position in an A2/AD environment will be a crucial warfighting requirement in the future, and conceptualizing various non-traditional sensors as possible sources of position information constitutes a modest first step in that direction.

THIS PAGE INTENTIONALLY LEFT BLANK

APPENDIX A: SOUND SPEED EQUATION CONSTANTS

C_{T1}	$0.50110939883\times10^{1}$
C_{T2}	$-0.550946843172\times10^{-1}$
C_{T3}	$0.221535969240\times10^{-3}$
C_{S1}	$0.132952290781\times10^{1}$
C_{S2}	$0.128955756844\times10^{-3}$
C_{P1}	$0.156059257041\times10^{0}$
C_{P2}	$0.244998688441\times10^{-4}$
C_{P3}	$-0.883392332513\times10^{-8}$
C_{TS}	$-0.127562783426\times10^{-1}$
C_{TP}	$0.635191613389\times10^{-2}$
C_{T2P2}	$0.265484716608\times10^{-7}$
C_{TP2}	$-0.159349479045\times10^{-5}$
C_{TP3}	$0.522116437235\times10^{-9}$
C_{T3P}	$-0.438031096213\times10^{-6}$
C_{S2P2}	$-0.161674495909\times10^{-8}$
C_{T2S}	$0.968403156410\times10^{-4}$
C_{TS2P}	$0.485639620015\times10^{-5}$
C_{TSP}	$-0.340597039004\times10^{-3}$

THIS PAGE INTENTIONALLY LEFT BLANK

LIST OF REFERENCES

[1] B. Peniston, *No Higher Honor: Saving the USS Samuel B. Roberts in the Persian Gulf.* Annapolis, Maryland: Naval Institute Press, 2006.

[2] H. Durrant-Whyte and T. Bailey, "Simultaneous localization and mapping: Part I," *IEEE Robotics & Automation Magazine,* pp. 99–108, Jun. 2006.

[3] M. Kaess, H. Johannsson, R. Roberts, V. Ila, J. Leonard and F. Dellaert, "iSAM2: Incremental smoothing and mapping with fluid relinearization and incremental variable reordering," *International Conference on Robotics and Automation,* Shanghai, China, 2011, pp. 3281.

[4] KN-6050 SEADeViL INS/DVL/GPS family. (n.d). Kearfott. [Online]. Available: http://www.kearfott.com/images/stories/pdf/DATASHEETS_KGN_NJ/SEA/kn-6050_seadevil.pdf. Accessed Sept. 15, 2014.

[5] WHOI acoustic communications: micro-modem. (2006). Woods Hole Oceanographic Institute. [Online]. Available: http://acomms.whoi.edu/umodem. Accessed Sept. 15, 2014.

[6] AUV modules: forward looking sonar, micro bathymetry, and gap fill. (2014). [Online]. Available: http://www.blueview.com/products/auv-modules-and-microbathymerty/component-auv-modules/. Accessed Sept. 15, 2014.

[7] V. A. Del Grosso, "New equation for the speed of sound in natural waters (with comparisons to other equations)," *Journal of the Acoustical Society of America,* vol. 56, no. 4, pp. 1084–1091, Oct. 1974.

[8] B. D. Dushaw, P. F. Worcester, B. D. Cornuelle, and B. M. Howe, "On equations for the speed of sound in seawater," *Journal of the Acoustical Society of America,* vol. 93, no. 1, pp. 255–275, Jan. 1993.

[9] "Introduction to the sonar equations," class notes for PH3401 Introduction to the sonar equations, Dept. of Physics, Naval Postgraduate School, Monterey, CA, Fall 2013.

[10] R. J. Urick, *Principles of Underwater Sound.* Los Altos, California: Peninsula Publishing, 1996.

[11] Sound paths. (n.d.). [Online]. Available: http://www.tpub.com/weather3/2-7.htm. Accessed Aug. 8, 2014.

[12] J. Colosi. (2013). Program to integrate the ray equations for 3 different environments. Unpublished.

[13] “The stochastic sonar equation,” class notes for OC3260 Fundamentals of ocean acoustics, Dept. of Oceanography, Naval Postgraduate School, Monterey, CA, 2012.

[14] Class notes for OC3260 Fundamentals of ocean acoustics, Dept. of Oceanography, Naval Postgraduate School, Monterey, CA, 2012.

[15] J. M. Walls and R. M. Eustice, “Experimental comparison of synchronous-clock cooperative acoustic navigation algorithms,” presented at the *OCEANS 2011*

[16] R. M. Eustice, L. L. Whitcomb, H. Singh and M. Grund, “Experimental results in synchronous-clock one-way-travel-time acoustic navigation for autonomous underwater vehicles,” in *Proceedings of the IEEE International Conference on Robotics and Automation,* Rome, Italy, 2007, pp. 4257.

[17] R. M. Eustice, H. Singh and L. L. Whitcomb, “Synchronous-clock, one-way-travel-time acoustic navigation for underwater vehicles,” *Jour. of Field Robotics*, vol. 28, no. 1, pp. 121–136, 2011.

[18] S. E. Webster, L. L. Whitcomb and R. M. Eustice, “Preliminary results in decentralized estimation for single-beacon acoustic underwater navigation,” in Zaragoza, Spain, 2010.

[19] S. E. Webster, R. M. Eustice, H. Singh and L. L. Whitcomb, “Advances in single-beacon one-way-travel-time acoustic navigation for underwater vehicles,” *International Journal of Robotics Research,* May 23, 2012.

[20] S. E. Webster, R. M. Eustice, H. Singh and L. L. Whitcomb, “Preliminary deep water results in single-beacon one-way-travel-time acoustic navigation for underwater vehicles,” presented at the International Conference on Intelligent Robots and Systems, St. Louis, Missouri, 2009, pp. 2053–2059.

[21] B. D. Dushaw, P. F. Worcester, B. D. Cornuelle, and B. M. Howe, “On equations for the speed of sound in seawater,” *Journal of the Acoustical Society of America,* vol. 93, no. 1, pp. 255–275, Jan. 1993.

[22] R. Smith, M. Self and P. Cheeseman, “Estimating uncertain spatial relationships in robotics,” Stanford Research Institute, 1990.

[23] A. Gelb, Ed., *Applied Optimal Estimation.* Cambridge, Massachusetts: MIT Press, 1974.

[24] R. E. Kalman, “A new approach to linear filtering and prediction problems,” *Journal of Basic Engineering*, vol. 82, pp. 35–45, 1960.

[25] M. Kaess, “Incremental smoothing and mapping,” Ph.D. dissertation, College of Computing, Georgia Institute of Technology, 2008.

[26] J. Neira and J. D. Tardos, “Data association in stochastic mapping using the joint compatibility test,” *IEEE Transactions on Robotics and Automation*, vol. 17, pp. 890, Dec. 2001.

[27] M. Kaess, A. Ranganathan and F. Dellaert, “iSAM: Incremental smoothing and mapping,” *IEEE Transactions on Robotics*, vol. 24, pp. 1365–1378, Dec. 2008.

[28] M. Walter and J. Leonard, “An experimental investigation of cooperative SLAM,” *Proc. of Intelligent Autonomous Vehicles*, Lisbon, Portugal, 2004.

[29] B. Kim, M. Kaess, L. Fletcher, J. Leonard, A. Bachrach, N. Roy and S. Teller, “Multiple relative pose graphs for robust cooperative mapping,” *Proc. IEEE International Conference on Robotics and Automatio*n, Anchorage, AK, 2010, pp. 3185–3193.

[30] D. Moratuwage, B. Vo and D. Wang, “A heirarchical approach to the multi-vehicle SLAM problem,” presented at the *15th International Conference on Information Fusion*, Singapore, Singapore, 2012, pp. 1119–1125.

[31] M. D. P. Moratuwage, W. S. Wijesoma, B. Kalyan, J. F. Dong, Namal Senarathne, P. G. C., F. S. Hover and N. M. Patrikalakis, “Collaborative multi-vehicle localization and mapping in marine environments,” presented at *OCEANS 2010,* Sydney, Australia, 2010.

[32] K. Y. K. Leung, T. D. Barfoot and H. H. T. Liu, “Decentralized cooperative simultaneous localization and mapping for dynamic and sparse robot networks,” presented at the *2010 IEEE/RSJ International Conference on Intelligent Robots and Systems*, Taipei, Taiwan, 2010, pp. 3554.

[33] E. D. Nerurkar and S. I. Roumeliotis, “Asynchronous multi-centralized cooperative localization,” presented at the *2010 IEEE/RSJ International Conference on Intelligent Robots and Systems,* Taipei, Taiwan, 2010, pp. 4352.

[34] A. Bahr, M. R. Walter and J. J. Leonard, “Consistent cooperative localization,” presented at the *2009 IEEE International Conference on Robotics and Automation*, Kobe, Japan, 2009, pp. 3415.

[35] M. Hua, T. Bailey, P. Thompson and H. Durrant-Whyte, “Decentralised solutions to the cooperative multi-platform navigation problem,” *IEEE Transactions on Aerospace and Electronic Systems*, vol. 47, no. 2, pp. 1433–1449, April 2011.

[36] J. M. Walls and R. M. Eustice, “An origin state method for lossy synchronous-clock acoustic navigation,” presented at *3rd IFAC Workshop on Navigation, Guidance, and Control of Underwater Vehicles*, Porto, Portugal, 2010.

[37] M. Erol, L. Vieira, A. Caruso, F. Paparella, M. Gerla and S. Oktug, “Multi stage underwater sensor localization using mobile beacons,” presented at *Second International Conference on Sensor Technologies and Applications*, Cap Esterel, France, 2008.

[38] A. Bahr, “Cooperative Localization for Autonomous Underwater Vehicles,” Ph.D dissertation, Joint Program in Applied Ocean Science and Engineering, Massachusetts Institute of Technology and Woods Hole Oceanographic Institute, 2009.

[39] A. Bahr, J. Leonard and A. Martinoli, “Dynamic positioning of beacon vehicles for cooperative underwater navigation,” *Proc. of IEEE Intelligent Robots and Systems*, Vilamoura, Portugal, 2012.

[40] J. Stipes, R. Hawthorne, D. Scheidt and D. Pacifico, “Cooperative localization and mapping,” *Proc. of IEEE international conference on networking, sensing and control*, Fort Lauderdale, FL, 2006, pp. 596–601.

[41] V. Pham and J. Juang, “A multi-robot, cooperative, and active slam algorithm for exploration,” *International Journal of Innovative Computing, Information, and Control*, vol. 9, pp. 2567–2583, Jun. 2013.

[42] C. S. Lee, D. E. Clark and J. Salvi, “SLAM with dynamic targets via single-cluster phd filtering,” *IEEE Journal of Selected Topics in Signal Processing*, vol. 7, no. 3, pp. 543–552, Jun. 2013.

[43] F. Abrate, B. Bona, M. Indri, S. Rosa and F. Tibaldi, “Multi-robot map updating in dynamic environments,” *Springer Tracts in Advanced Robotics*, vol. 83, pp. 147, 2013.

[44] A. W. Stroupe, M. C. Martin and T. Balch, “Merging gaussian distributions for object localization in multi-robot systems,” in *Experimental Robotics VII*, D. Rus and S. Singh, Eds. Springer Berling Heidelberg, 2001, pp. 343–352.

[45] L. Paull, M. Seto and J. J. Leonard, “Decentralized cooperative trajectory estimation for autonomous Underwater vehicles,” presented at *IEEE International Conference on Intelligent Robots and Systems*, Chicago, IL, 2014.

INITIAL DISTRIBUTION LIST

1. Defense Technical Information Center
   Ft. Belvoir, Virginia

2. Dudley Knox Library
   Naval Postgraduate School
   Monterey, California